JCI The Journal of Clinical Investigation

Blocking endothelial apoptosis revascularises the retina in a model of ischemic retinopathy

Zoe L. Grant, … , Robert C.A. Symons, Leigh Coultas

J Clin Invest. 2020. https://doi.org/10.1172/JCI127668.

Research In-Press Preview Angiogenesis

Graphical abstract

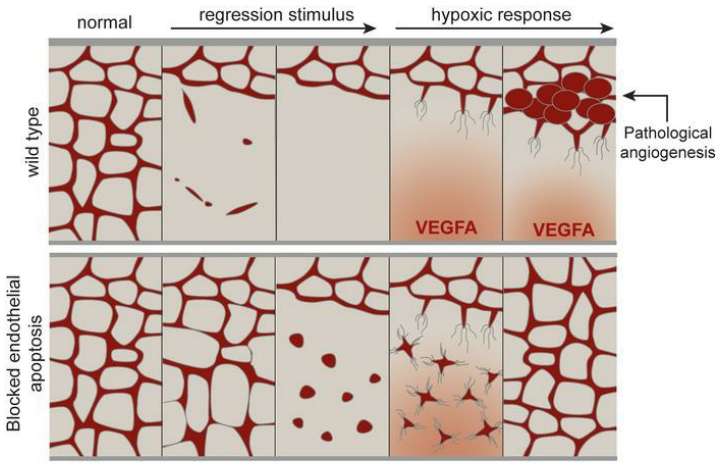

Blocking endothelial apoptosis revascularises the retina in a model of ischemic retinopathy

Zoe L. Grant[1,2], Lachlan Whitehead[1,2], Vickie H. Y. Wong[3], Zheng He[3], Richard Y. Yan[1], Abigail R. Miles[1], Andrew V. Benest[4], David O. Bates[4], Claudia Prahst[5], Katie Bentley[5,6,7], Bang V. Bui[3], Robert C. A. Symons[3,8,9] & Leigh Coultas[1,2]

[1]The Walter and Eliza Hall Institute of Medical Research, 1G Royal Parade, Parkville, Victoria 3052, Australia

[2]Department of Medical Biology, University of Melbourne, 1G Royal Parade, VIC 3052 Australia

[3]Department of Optometry and Vision Sciences, University of Melbourne, Parkville, 3010 Australia

[4]Centre for Cancer Sciences, Biodiscovery Institute, School of Medicine, University of Nottingham NG7 2RD, UK and COMPARE University of Birmingham and University of Nottingham Midlands, UK

[5]Center for Vascular Biology Research, Beth Israel Deaconess Medical Center, Harvard Medical School, Boston, MA 02215, USA

[6]Department of Biomedical Engineering, Boston University, MA

[7]Beijer Laboratory for Gene and Neuroscience Research, Department of Immunology, Genetics and Pathology, University of Uppsala, 751 85 Uppsala, Sweden

[8]Department of Surgery, University of Melbourne, Parkville, 3010 Australia

[9]Department of Ophthalmology, Royal Melbourne Hospital, Parkville, 3050 Australia

Address correspondence to:

Leigh Coultas, Epigenetics and Development Division, The Walter and Eliza Hall Institute of Medical Research, 1G Royal Parade, Parkville, Vic, 3052 Australia

Ph (+61) 3 9345 2860, Email: lcoultas@wehi.edu.au

Competing Interests

The authors have declared that no conflict of interest exists.

Abstract

Aberrant, neovascular retinal blood vessel growth is a vision-threatening complication in ischemic retinal diseases. It is driven by retinal hypoxia frequently caused by capillary non-perfusion and endothelial cell (EC) loss. We investigated the role of EC apoptosis in this process using a mouse model of ischemic retinopathy, in which vessel closure and EC apoptosis cause capillary regression and retinal ischemia followed by neovascularisation. Protecting ECs from apoptosis in this model did not prevent capillary closure or retinal ischemia. Nonetheless, it prevented the clearance of ECs from closed capillaries, delaying vessel regression and allowing ECs to persist in clusters throughout the ischemic zone. In response to hypoxia, these preserved ECs underwent a vessel sprouting response and rapidly reassembled into a functional vascular network. This alleviated retinal hypoxia, preventing subsequent pathogenic neovascularisation. Vessel reassembly was not limited by VEGFA neutralisation, suggesting it was not dependent on the excess VEGFA produced by the ischemic retina. Neutralisation of ANG2 did not prevent vessel reassembly, but did impair subsequent angiogenic expansion of the reassembled vessels. Blockade of EC apoptosis may promote ischemic tissue re-vascularisation by preserving ECs within ischemic tissue that retain the capacity to reassemble a functional network and rapidly restore blood supply.

Introduction

Angiogenesis is the growth of new blood vessels from pre-existing vessels and occurs through a tightly regulated response of endothelial cells (ECs) to pro-angiogenic factors (1, 2). Insufficient vascular supply, which may arise due to impaired vessel growth (3), capillary loss (4) or vessel obstruction (5), causes tissue ischemia. While increased angiogenesis correlates with better outcomes in ischemic diseases like stroke (6), ischemia and the upregulation of VEGFA can drive aberrant angiogenesis exacerbating certain diseases. This is particularly evident in retinal diseases, such as proliferative diabetic retinopathy, retinal vein occlusion and retinopathy of prematurity where aberrant angiogenesis (neovascularisation) increases the risk of severe vision loss and blindness (7). Current treatments for neovascular disease in the retina revolve around reducing the angiogenic stimulus either by decreasing the metabolic activity of the retina or by direct inhibition of VEGFA (8-12). While these approaches improve visual outcomes, many patients show either no or a sub-optimal response (8, 9). Capillary regression and the loss of ECs from the microvasculature is commonly associated with progression to neovascular disease in the retina and can occur in response to metabolic dysregulation (4), hyperoxia (13), or interrupted blood flow (14, 15). ECs die by apoptosis, a genetically programmed form of cell death (16), in settings where extensive vessel regression occurs (17, 18). Retinal capillaries in patients with diabetic retinopathy for example show elevated levels of EC apoptosis prior to progression to the proliferative phase (4, 19). Understanding the role of apoptosis in EC loss and vessel regression leading to retinal ischemia may therefore provide new insight into vascular changes associated with ischemia and potentially new avenues for preventing disease progression.

Apoptosis is regulated by two pathways, one consisting of BCL2 family proteins, the other by cell surface 'death receptors'. Previous studies have demonstrated a key role for the BCL2 family of proteins in the regulation of EC apoptosis (17). The BCL2 family consists of opposing factions of pro-survival and pro-apoptotic members (16), the balance of which determines whether the apoptosis effector proteins BAK and BAX become activated (20). Previous studies have shown that among the BCL2 family, the pro-survival protein MCL1 (21), the pro-apoptotic protein BIM (22, 23), and the two effector proteins BAK and BAX (24) have a central role in regulating EC apoptosis in the retina in vivo.

Vessel regression is a normal process necessary for establishing hierarchic vessel patterning during angiogenesis and the removal of redundant or damaged vascular networks (17, 18). During angiogenic vessel remodelling, local differences in blood flow shear between neighbouring vessel segments determines which will be 'pruned' away (25-27). This selective vessel pruning is driven by EC migration (25, 27, 28), does not cause ischemia and does not require EC apoptosis (24). In contrast, apoptosis does appear responsible for capillary regression in other contexts, including those that leave tissues with insufficient vascular supply, causing ischemia. Exactly how apoptosis contributes to vessel loss in this context and the outcomes of preventing it are not well understood.

Here we have investigated the effect of blocking EC apoptosis in a mouse model of ischemia-induced neovascular disease (4), in which blocking apoptosis is known to prevent capillary loss and subsequent neovascularisation (23). Our results show that EC apoptosis in this model is secondary to a vessel closure event that deprives downstream capillaries of blood flow. Rather than preventing this vessel closure or subsequent vessel degeneration, protecting ECs from apoptosis instead preserved ECs from these closed vessels within the

ischemic region that were capable of rebuilding a functional vascular network in response to hypoxia-derived signals, restoring tissue oxygenation and mitigating the damaging effects of prolonged hypoxia on the retina.

Results

Blocking BCL2 pathway apoptosis results in EC survival and delayed vessel regression

To determine whether EC apoptosis was responsible for vessel regression causing ischemia, we investigated its role in the oxygen-induced retinopathy (OIR) model (29) (Supplementary Figure 1A). In this model, transient exposure of mice to high oxygen causes the apoptotic death of ECs and consequent regression of retinal capillaries in the centre of the retina, resulting in relative retinal hypoxia once the mice are returned to room air oxygen levels. This is followed by the development of abnormal vascular lesions that resemble those found in neovascular retinal diseases (4) and was developed as a model of retinopathy of prematurity. To block apoptosis, we used mice that we previously generated, in which apoptosis was inactivated in ECs through combined deletion of BAK and BAX ($Bak^{-/-}Bax^{EC/EC}$ mice (24)). $Bak^{-/-}Bax^{EC/EC}$ mice lack BAK in all tissues and BAX only in ECs, a necessary strategy because $Bak^{-/-}$ mice are viable, whereas most $Bak^{-/-}Bax^{-/-}$ double null mice die at birth due to a range of birth defects (30). Relevant to the age of mice studied here, $Bak^{-/-}Bax^{EC/EC}$ mice develop a normal retinal vascular network in the first few weeks following birth (24). After 24 h of exposure to high oxygen, control genotype mice contained extensive numbers of apoptotic ECs (active caspase 3^+ $PECAM1^+$ cells). In contrast, retinas from $Bak^{-/-}Bax^{EC/EC}$ mice were almost completely devoid of apoptotic ECs after 24 or 48 h of oxygen exposure (Figure 1A & B). By contrast, other forms of programmed cell death, namely death receptor mediated apoptosis (caspase-8-dependent) and MLKL-dependent necroptosis were dispensable for vaso-obliteration as $casp8^{-/-}Mlkl^{-/-}$ double-knockout mice underwent normal vaso-obliteration when exposed to high oxygen

(Supplementary Figure 1B & C). These results confirm the central role of the BCL2-regulated apoptosis pathway in the apoptotic response of ECs in the OIR model.

As a result of blocking apoptosis, *Bak*$^{-/-}$*Bax*$^{EC/EC}$ retinas contained significantly more vasculature than control littermates following 24 - 48 h of high oxygen exposure (Figure 1C, Supplementary Figure 1D). Despite this, the vessel area in *Bak*$^{-/-}$*Bax*$^{EC/EC}$ retinas declined with increasing duration of high oxygen exposure (Figure 1D). This loss of vasculature was due to vessel regression based on the reduced occupancy of collagen IV+ vascular basement membranes with PECAM1^{+} ECs (31) (Figure 1E & F, Supplementary Figure 1E). By 48 h of exposure to high oxygen, ongoing vessel regression had caused the network in *Bak*$^{-/-}$*Bax*$^{EC/EC}$ retinas to degenerate into isolated vessel fragments and endothelial clusters that in many cases remained linked by empty collagen IV sleeves (Figure 1E & G), evidence that they were once part of an interconnected vascular network.

The *Tie2-cre* transgene used to generate *Bak*$^{-/-}$*Bax*$^{EC/EC}$ mice is active in hematopoietic cells as well as ECs. The *Cdh5-CreERT2* transgene (32) is active in ECs but not hematopoietic cells following postnatal administration of tamoxifen (21). Postnatal deletion of *Bax* only from ECs using this cre (*Bak*$^{-/-}$*Bax*$^{iEC/iEC}$ mice) recapitulated the fragmented vascular phenotype after 48 h of high oxygen exposure (Supplementary Figure 1F-H). This result confirmed that the fragmented vascular phenotype is due to apoptosis blockade specifically in ECs. Therefore, blocking apoptosis in ECs does not prevent vessel regression triggered by exposure to high oxygen.

EC apoptosis-independent loss of blood flow precedes vessel regression

We sought to determine why apoptosis suppression could not prevent the loss of retinal capillary network integrity following high oxygen exposure by investigating the causes of EC apoptosis and vessel regression. VEGFA promotes EC survival via the BCL2 pathway (33, 34). It is down-regulated during exposure to high oxygen and this has been suggested to contribute to vessel regression in the OIR model (35-37). VEGFR2 is the major VEGFA receptor responsible for survival signalling by VEGFA (38). Using tamoxifen-inducible, EC-specific *Vegfr2* mutants described previously (39), we found that reducing VEGFR2 through tamoxifen administration from postnatal day (P)7 (the age at which retinal vessels are susceptible to high oxygen) did not result in widespread loss of central retina capillaries when analysed at P10 (Supplementary Figure 2A & B). This result suggests that a reduction in VEGFA activity alone is not sufficient to replicate the vaso-obliteration that occurs in the OIR model and is consistent with previous findings (40, 41).

Reduced blood flow triggers the regression of immature retinal vessels (28, 41) and EC apoptosis in OIR has previously been proposed to occur secondary to loss of blood flow (41, 42). Widespread EC apoptosis was evident in control mice but not $Bak^{-/-}Bax^{EC/EC}$ mice 8 h after onset of exposure to high oxygen (Supplementary Figure 2C & D). With few exceptions, apoptosis was localised to non-perfused vessels based on co-staining for active caspase 3 and intravenously perfused *L. esculentum* lectin (Supplementary Figure 2E), which binds to and marks ECs in patent vessels. Loss of flow was mostly observed downstream of arterial side-branches that had closed (Figure 2A). This pattern of vessel closure was observed in both control and $Bak^{-/-}Bax^{EC/EC}$ mice (Figure 2A). The number of perfused arterial side branches remaining at 8 h was not different between $Bak^{-/-}Bax^{EC/EC}$

mice and controls (Figure 2A & B). This demonstrates that apoptosis is not responsible for hyperoxia-induced arterial side-branch closure or deprivation of downstream capillaries of blood flow. Nonetheless, the regression of closed arterial side-branches was delayed in the absence of apoptosis as fewer non-perfused side-branches in the *Bak*$^{-/-}$*Bax*$^{EC/EC}$ mice had fully disconnected their lumens from the artery by 8 h (Supplementary Figure 2F & G). There was also less regression occurring in non-perfused *Bak*$^{-/-}$*Bax*$^{EC/EC}$ capillaries relative to controls (Figure 2C & D), although the non-perfused capillaries in mutants still showed slightly elevated levels of regression relative to the peripheral capillary plexus region that is unaffected by high oxygen exposure (Figure 2D).

Retinas vaso-obliterated by exposure to high oxygen become hypoxic on return to room air owing to the loss of the central capillary network (43) and this was observed in control mice following either 24 or 48 h of exposure to high oxygen (Figure 2E & F). The extent of hypoxia in littermate *Bak*$^{-/-}$*Bax*$^{EC/EC}$ retinas was equivalent to the controls, consistent with loss of blood flow to and fragmentation of the central retinal capillaries (Figure 2E & F). These data suggest that vessel regression still occurs in the absence of apoptosis, likely as a result of blood flow loss.

Preserved Bak*$^{-/-}$*Bax*$^{EC/EC}$ *ECs rapidly reassemble the vessel network in response to hypoxia

In WT mice, the onset of hypoxia following return to room air induces a sprouting angiogenic response from the remaining vasculature that gradually revascularises the central retina through centripetal growth of the network (44, 45). To determine whether the preserved ECs in the central retina of *Bak*$^{-/-}$*Bax*$^{EC/EC}$ mice could also respond to hypoxia,

mice were exposed to high oxygen for 48 h to fragment the vascular network, returned to room air to induce hypoxia in the avascular retina, then examined 24 h later (referred to as 48 + 24 RA) (Supplementary Figure 3A). As expected, new vessel growth from the peripheral plexus and radial veins in control mice only partially revascularised the retina 24 h after onset of hypoxia (Figure 3A, B & C). In contrast, *Bak*$^{-/-}$*Bax*$^{EC/EC}$ retinas showed a significant increase in vessel area accompanied by the cessation of vessel regression and reestablishment of an interconnected vascular network (Figure 3A, C - F).

To understand how an intact vascular network was re-established in the *Bak*$^{-/-}$*Bax*$^{EC/EC}$ mice, we performed time-lapse imaging to track the fate of the preserved ECs. For this, the Cre-inducible, cell membrane-targeted EGFP reporter allele *mTmG* (46) was intercrossed with the tamoxifen-inducible *Bak*$^{-/-}$*Bax*$^{iEC/iEC}$ mice. Following tamoxifen administration, *Bak*$^{-/-}$*Bax*$^{iEC/iEC}$*mTmG*$^{ki/+}$ pups were exposed to high oxygen for 48 h, returned to room air for 12 h to initiate the hypoxic response, then retinas were explanted and immediately time-lapse imaged at 30 min intervals for 5 h (Supplementary Figure 3B & C). Time-lapse imaging showed that ECs in the isolated clusters adopted a migratory phenotype consistent with tip cell activity normally seen during sprouting angiogenesis (1). Through this, the isolated ECs actively re-established connections with their neighbours, reassembling the network (Figure 3G, Supplementary Movie 1-3, black arrows). Vessel sprouts establishing new connections were also observed from already intact vessels (Supplementary Movie 1 & 2, red arrows). In many cases, migrating ECs extended multiple filopodial projections suggesting de novo pathfinding similar to the sprouting angiogenesis seen in control mice (Figure 3H, Supplementary Movie 3, red arrows). In other cases, ECs appeared to track along pre-determined paths (Supplementary Movie 3, blue arrows). These data show that

isolated EC clusters protected from apoptosis are active participants in the reestablishment of an intact vascular network during revascularisation of the ischemic retina.

During normal sprouting angiogenesis in the retina, new vessel growth is coupled to EC proliferation (47). Control and *Bak*$^{-/-}$*Bax*$^{EC/EC}$ retinas were stained for phospho-histone H3(Ser10) to identify proliferating ECs 24 h after return to room air. In control retinas, EC proliferation accompanied regrowth of the central retinal vasculature (Figure 4A & B, Supplementary Figure 3D). In contrast, reassembling vessels in the centre of *Bak*$^{-/-}$*Bax*$^{EC/EC}$ retinas contained few proliferating ECs (Figure 4A & B). EC proliferation in the peripheral vasculature was similar between control and *Bak*$^{-/-}$*Bax*$^{EC/EC}$ mice, indicating that there was not a general EC proliferation defect in the mutants (Supplementary Figure 3E).

To determine whether EC number changed during the process of regression and reassembly, we quantified EC number in normal (normoxic), fragmented (48 h high O_2) and reassembled (48 + 24 RA) *Bak*$^{-/-}$*Bax*$^{EC/EC}$ central retina vessels, using EC nuclei markers FLI1 and ERG. FLI1 was down-regulated in ECs of fragmented vessels (Supplementary Figure 3F), therefore ERG was used to quantify EC number under this condition. We found that the number of ECs in the central retina of *Bak*$^{-/-}$*Bax*$^{EC/EC}$ mice remained constant between normoxic, fragmented and reassembled vessels (Figure 4C & D). Collectively, these data show that blocking apoptosis prevents the loss of ECs from the retina and that reassembly of these cells back into interconnected vessels does not require the production of new ECs.

The extent of network fragmentation influences vessel reassembly

The degree of network fragmentation in *Bak*$^{-/-}$*Bax*$^{EC/EC}$ mice was proportional to the time spent in the high oxygen environment. Those mice exposed to high oxygen for 24 h showed less extensive vessel regression and network fragmentation than those exposed for 48 h (Figure 1F & G, Supplementary Figure 4A). When mice exposed to high oxygen for 24 h were returned to room air for a further 24 h to stimulate hypoxia-driven vessel reassembly (24 + 24 RA), the vascular area, vessel width and network branch points were all closer to that of mice raised in normoxia than was observed in the *Bak*$^{-/-}$*Bax*$^{EC/EC}$ mice exposed to 48 + 24 RA (Supplementary Figure 4 B – D). This finding suggests that the sooner tissue hypoxia manifests after flow interruption, the more efficiently apoptosis-resistant ECs can reassemble a functional vascular network.

Vessel reassembly facilitated by the blocking of apoptosis reverses retinal hypoxia, and associated pathological responses

To assess whether reassembled vessels were functional, we investigated vessel perfusion and retinal hypoxia in *Bak*$^{-/-}$*Bax*$^{EC/EC}$ and control mice subjected to 48 + 24 RA. Lectin perfusion showed that most reassembled vessels in *Bak*$^{-/-}$*Bax*$^{EC/EC}$ retinas were patent and perfused 24 h after return to room air (Figure 5A). Consistent with this, there was significantly less hypoxia in the central retinas of *Bak*$^{-/-}$*Bax*$^{EC/EC}$ mice compared to similarly treated controls (Figure 5B & C). These mice also displayed less retinal hypoxia than *Bak*$^{-/-}$*Bax*$^{EC/EC}$ retinas still in the fragmented state immediately following exposure to 48 h of high oxygen alone (Figure 5B & C). Retinal hypoxia in the OIR model following return to room air results in increased expression of VEGFA (36, 48). Accordingly, VEGFA protein levels increased substantially in control mice 24 h after return to room air, but this was

significantly reduced in *Bak*$^{-/-}$*Bax*$^{EC/EC}$ retinas (Figure 5D). This was consistent with there being less hypoxia due to reassembly of the vascular network and restoration of the vascular supply. As neovascular lesion formation is dependent on VEGFA (44, 45, 49), we assessed whether the reduction in hypoxia-induced VEGFA brought about by vessel reassembly would also translate to a reduction in neovascular lesion formation. Neovascular lesions have a glomerular vessel structure, distinct from the normal branched vessel network pattern. These lesions stained brightly for the basement membrane protein collagen IV (Figure 5G, PECAM1 signal). The strong contrast in collagen IV signals between normal and neovascular vessels enabled us to quantify neovascular lesions as bright, globular collagen IV structures. Whereas control mice exposed to high oxygen and returned to room air for 5 days developed extensive neovascular lesion area, this was significantly reduced in *Bak*$^{-/-}$*Bax*$^{EC/EC}$ retinas (Figure 5E – H). Additionally, Müller cell gliosis, an indicator of retinal stress, was significantly reduced in *Bak*$^{-/-}$*Bax*$^{EC/EC}$ mice compared to the controls (Figure 5I & J). These findings demonstrate that reassembled vessel networks are functional and prevent pathological consequences of prolonged tissue hypoxia in the retina.

Reducing VEGFA levels does not prevent vessel reassembly or its suppression of neovascular lesion formation

As elevated VEGFA drives aberrant angiogenesis in ischemic retinas, we investigated whether it was also necessary for the vessel reassembly that occurred in the absence of EC apoptosis. To test this, *Bak*$^{-/-}$*Bax*$^{EC/EC}$ mice were exposed to 48 + 24 RA to induce network fragmentation and reassembly and administered with either a VEGFA neutralising

antibody (50) or isotype control on return to room air (Figure 6A). VEGFA neutralisation did not appear to prevent vessel reassembly as no difference was observed in central retinal vascular area between mice treated with anti-VEGFA or isotype control antibody (Figure 6B & C). Supporting this, the hypoxic area in the central retina was not different in *Bak*$^{-/-}$ *Bax*$^{EC/EC}$ mice treated with anti-VEGFA or isotype control antibody (Figure 6D). We confirmed that the systemically delivered antibodies were neutralising VEGFA in the retinal vessels by staining for ESM1 (Supplementary Figure 5A-C). The expression of ESM1 is dependent on VEGFA (51). Vessel reassembly proceeded in anti-VEGFA treated mice even under conditions of high VEGFA signalling inhibition, in which ESM1 expression was reduced by 94% (Supplementary Figure 5A-E). VEGFA inhibition under conditions that reduced neovascular lesion area by 50% in control genotype mice did not interfere with the ability of vessel reassembly to prevent neovascular lesion formation 5 days after return to room air (Figure 6E – G). In contrast, vessel reassembly in *Bak*$^{-/-}$ *Bax*$^{EC/EC}$ mice was effective at reducing neovascular area by 88% (Figure 6G).

The mature retinal vasculature consists of three layers: superficial, middle and deep. *Bak*$^{-/-}$*Bax*$^{EC/EC}$ mice had established more extensive vessel networks in these layers than control mice 5 days after return to room air, evident from the extent of vaso-obliterated area repair (Figure 6F & H) and the vessel area in these layers (Supplementary Figure 5F – H). None of this was affected when VEGFA was neutralised in mice of either genotype (Figure 6H and Supplementary Figure 5 F – H). Taken together, these data show that vessel reassembly in the absence of EC apoptosis is not dependent on abnormally high VEGFA levels or impeded when VEGFA levels are reduced to a level sufficient to suppress aberrant neovascularisation or ESM1 expression.

Reducing ANG2 does not prevent vessel reassembly, but does impair angiogenic expansion of reassembled vessels

Our data show that vessel reassembly occurs in response to hypoxia by cells that exhibit hallmark features of endothelial tip cells. ANG2 is highly expressed in tip cells (52-54) and is essential for sprouting angiogenesis in the retina (53, 55, 56). ANG2 is upregulated in ECs by hypoxia (57-60), including in the OIR model (57). Given this, we sought to determine whether ANG2 was necessary for vessel reassembly. To investigate ANG2 expression in reassembling vessels, control and *Bak*$^{-/-}$*Bax*$^{EC/EC}$ mice were exposed to high oxygen for 48 h, returned to room air for 12 or 24 h and then stained for ANG2. As expected, ANG2 expression in control mice was strongly upregulated in ECs along the sprout front adjacent to the avascular central retina at both time points (Figure 7A). As previously reported for this antibody (61, 62), ANG2 was expressed preferentially in ECs located at the sprout front consistent with tip cell identity (Supplementary Figure 6A). In *Bak*$^{-/-}$*Bax*$^{EC/EC}$ mice we found strong ANG2 expression in the reassembling endothelium in the central retina 12 h after return to room air (Figure 7B). By 24 h, when most reassembly was complete, only a few patches of ECs with strong ANG2 expression remained (Figure 7B, yellow arrows).

To test whether ANG2 was necessary for vessel reassembly, *Bak*$^{-/-}$*Bax*$^{EC/EC}$ mice were exposed to 48 + 24 RA to induce network fragmentation and reassembly and administered with either an ANG2 neutralising antibody (63) or an isotype control antibody on return to room air (Figure 7C). No difference was observed in the central retina vessel area or network fragmentation between treatment groups in the *Bak*$^{-/-}$*Bax*$^{EC/EC}$ mice, suggesting

ANG2 inhibition did not inhibit vessel reassembly (Figure 7D - F). ANG2 inhibition did however reduce endothelial tip cell activity in the retina. Wild type mice treated with ANG2 neutralising antibody following return to room air showed a 65% reduction in tip cells based on the morphological criteria of filopodial clusters (Supplementary Figure 6B & C), consistent with the known role of ANG2 in promoting tip cell activity in the retina (53). Consistent with this, ANG2 inhibition prevented the formation of new vessel networks from the reassembled vessels by sprouting angiogenesis. Whereas extensive superficial and mid layer vasculature was present in ANG2 inhibited $Bak^{-/-}Bax^{EC/EC}$ retinas 5 days after return to room air as a result of vessel reassembly (Figure 7G & H), these animals contained less deep layer vasculature compared to isotype control treated mice (Figure 7G - I). Deep layer vessels form from vessel sprouts that emerge from the superficial layer. We observed strong ANG2 expression in these sprouts in the periphery of $Bak^{-/-}Bax^{EC/EC}$ retinas 24 h after return to room air (Figure 7B, pink arrows) and formation of these vessels during normal retinal development is impaired in *Ang2* mutants (55, 56). Taken together, these data suggest that ANG2 is not required for the initial process of vessel reassembly, but is required for further expansion of the reassembled vessels by sprouting angiogenesis.

Discussion

While blocking apoptosis has previously been shown to prevent neovascularisation in the OIR model (23), the way it did so was unknown. We show that protecting against BAK/BAX-dependent apoptosis did not prevent the initial loss of perfusion or breakdown of the vasculature through vessel regression that leads to areas of the retina becoming ischemic. Rather, it allowed those ECs that would ordinarily die during the process of vessel regression to survive and persist. These did not persist as intact or functional vessels, but instead as isolated clusters of cells scattered throughout the ischemic zones. As the tissue surrounding these isolated ECs became hypoxic, they underwent a sprouting angiogenic response. Through this, they re-established connections with each other and neighbouring vessels, reassembling into a functional network. These reassembled vessels rapidly restored oxygen supply to the ischemic tissue, thereby diminishing hypoxia-induced pathological responses (Supplementary Figure 6D). Our data show this mechanism replaces vessels sooner than normal angiogenesis would, which must grow a new network (including replacement ECs lost to apoptosis during vaso-obliteration) from vessels peripheral to the ischemic lesion (Supplementary Figure 6D).

We found that ischemia in the OIR model was caused by EC apoptosis-independent vessel closure, predominantly in arterial side-branch vessels. Vessel closure in the OIR model has been shown to depend on DLL4/Notch signalling through the regulation of vasoactive gene expression (41). Arterial side-branch closure led to the loss of blood flow to downstream capillaries, suggesting that loss of blood flow shear constitutes the major initiating event in vaso-obliteration. Previous studies have suggested vessel closure occurs prior to apoptosis (41, 42). When apoptosis was blocked, capillaries deprived of blood flow

still initiated a vessel regression response in which vessels disassembled and ECs retracted into isolated clusters resulting in network fragmentation. The vessel regression seen in the absence of apoptosis likely involves a process of cell migration similar to that which occurs in normal angiogenic vessel pruning. That process also occurs in response to blood flow changes (25-28) and is independent of EC apoptosis (24).

When protected from apoptosis, ECs in the fragmented, non-perfused vessels retained the capacity to initiate a sprouting angiogenesis phenotype. This occurred in response to hypoxia. These cells displayed behavioural and morphological features typical of endothelial tip cells that guide the growth of new vessels during sprouting angiogenesis (64). This process is responsible for the vascularisation of the retina in response to physiologic hypoxia (1, 65). Through this behaviour, the isolated cells were able to re-establish connections with neighbouring vessels and reassemble into a functional network. In some instances, ECs appeared to migrate along pre-determined paths. Empty vascular basement membranes left behind during vessel regression can act as a scaffold for vessel regrowth (66, 67). It is likely this was occurring during vessel reassembly as the PECAM1:collagen IV ratio returned to normal during vessel reassembly, suggesting it involves at least to some extent, recanalization of empty basement membranes.

Unlike normal sprouting angiogenesis in which EC proliferation is coupled to new vessel growth (47), the sprouting and network reassembly we observed in the absence of apoptosis proceeded largely without the need for EC proliferation. While the exact reasons for this lack of proliferation are unclear, the unchanging number of ECs throughout the process of network fragmentation and reassembly possibly suggests some form of negative feedback mechanism on proliferation. Additionally, many of the reassembling ECs showed

morphological and molecular features consistent with tip cell activity/identity, a state known to have less proliferative activity than other EC types (64). Nonetheless, the formation of extensive deeper layer vasculature suggests reassembled vessels retain the capacity for further network growth that likely does require EC proliferation. Deep layer retinal vessels grow from vessel sprouts originating from the superficial vascular layer and have not yet formed when mice start the OIR procedure. These vessels therefore do not reassemble from existing EC clusters in the apoptosis-resistant mutants in the same way the superficial layer does. The presence of deep layer vasculature in $Bak^{-/-}Bax^{EC/EC}$ mice 5 days after return to room air therefore suggests that reassembled superficial layer vessels are competent to undergo further sprouting angiogenesis to give rise to the new vessel networks in the deeper layers. These vessels are important for normal retina function as defects in their formation are associated with diseases causing vision loss (68).

Vessel reassembly occurred in response to hypoxia, prompting us to investigate whether it was dependent on the hypoxia-induced, pro-angiogenic growth factors VEGFA and ANG2. Both VEGFA and ANG2 are upregulated in the OIR model following the onset of hypoxia (36, 48, 57) and are required for pathological neovascular lesion formation (44, 45, 49, 69). Our data show that reducing VEGFA to levels that suppress pathological angiogenesis did not interfere with the vessel reassembly that occurs in the absence of EC apoptosis. While these findings do not necessarily exclude a role for low-level VEGFA in the reassembly process, they do show that it can proceed at levels of VEGFA that are limiting for pathological angiogenesis, or reduce ESM1 expression by 94%. While the effects of VEGFA neutralising antibodies on neovascularisation and ESM1 expression we observe suggest direct inhibition in the retina based on other experimental evidence (44,

45, 49, 51), we cannot rule out systemic effects following intraperitoneal administration of the neutralizing antibodies.

ANG2 is a pro-angiogenic growth factor expressed in endothelial tip cells (52-54). It is essential for sprouting angiogenesis in the retina (53, 55, 56). Despite the fact that ANG2 was upregulated in the ECs of reassembling vessels, neutralisation of ANG2 did not prevent vessel reassembly. ANG2 was however required for reassembled vessels to undergo subsequent angiogenic expansion to form deep layer vasculature. The requirement for ANG2 in the formation of deep layer vessels has been previously demonstrated in the context of normal, developmental retinal angiogenesis (55, 56). While we cannot rule out the possibility that some level of ANG2 activity is required for vessel reassembly, our results suggest the threshold is lower than that needed for normal sprouting angiogenesis. While the effects of ANG2 neutralisation on tip cell activity, sprouting angiogenesis and deep layer vessel formation match previous genetic and inhibitor-based studies *in vivo* (53, 55, 56) and *in vitro* (70, 71) and suggest direct neutralisation of ANG2 in the retina, we cannot rule out systemic effects following intraperitoneal administration of the neutralizing antibodies. We also cannot rule out the possibility that vessel reassembly occurs before the full effect of ANG2 or VEGFA neutralising antibodies manifests. However vessel reassembly became less efficient following longer exposure to high oxygen, and VEGFA and ANG2 neutralisation still did not prevent reassembly even following longer (3 days) exposure to high oxygen.

Sprouting angiogenesis and tip cell activity are regulated by many signalling inputs in addition to VEGFA and ANG2. These include BMPs, FGFs, Notch, cell adhesion and direct hypoxia sensing among others (72), any of which may be essential during the vessel

reassembly process. In addition to forming new vessel sprouts indicative of tip cell activity, vessel reassembly also appeared to involve recanalization of pre-existing basement membranes. This process may not be as dependent on factors involved in normal sprouting angiogenesis and may point to the requirement of other pathways, the identity of which will require further investigation.

The reassembly of vessel fragments we observed bears similarities to vessel formation in other contexts. During vasculogenesis, angioblasts coalesce into endothelial cords before establishing lumenised vessels (2); isolated clusters of lymphatic ECs incorporate into growing lymphatic vessel networks (73); and isolated vessel segments in the rat mesentery reconnect during network growth (74). We showed that isolated ECs protected from apoptosis driven by BAK and BAX can respond to hypoxic stimuli to reassemble themselves into a functional vessel network, resulting in rapid network repair and tissue reoxygenation. This had the effect of reducing hypoxia, pathological neovascularisation and reactive retinal gliosis. Manipulation of other pathways, such as ANG1 (44) and ATM signalling (75), have also been shown to accelerate the repair of the retinal network and reduce neovascularisation in the OIR model. In these cases, vaso-obliteration proceeded normally and enhanced centripetal growth of the peripheral vascular network accounted for the vessel repair and took longer than the reassembly process we describe (44, 75). Blocking apoptosis in the OIR model therefore enabled a fundamentally different and faster approach for restoring blood supply to the ischemic retina.

Network reassembly became less efficient the longer ECs were exposed to high oxygen and therefore in the fragmented, flow-deprived state. While this reduced efficiency may simply reflect the fact that more fragmentation had occurred at these later time points,

taking longer to repair, other factors may contribute to hinder the process. By 48 h, ECs had down-regulated the transcription factor FLI1 and may down-regulate other genes that may affect their responsiveness to angiogenic stimuli. Changes to the neurovascular unit over time likely also affect reassembly. Astrocytes promote retinal angiogenesis both in normal development (37) and vessel regrowth in the OIR model (44, 76). The astrocyte network deteriorates rapidly beyond 24 h of exposure to high oxygen (77). This may explain why revascularisation in our model was less efficient, but still effective, beyond 24 h of high oxygen exposure.

Current treatments for neovascular disease in the retina revolve around reducing the angiogenic stimulus. This is done either by decreasing the metabolic demand of the retina or direct inhibition of VEGFA (8-12). Our findings show that in the OIR model for retinopathy of prematurity, preventing EC apoptosis can accelerate revascularisation of the retina and reduce the hypoxic stimulus that drives abnormal VEGFA expression. Our data show that protecting ECs from apoptosis in this model enables them to persist within ischemic tissue without the need for ongoing blood flow support and reestablish functional vessels sooner than normal angiogenic growth can achieve. Furthermore, like VEGFA inhibition, blocking apoptosis in the OIR model was effective at preventing subsequent neovascular response. These findings may also have implications for restoring blood flow in other ischemic retinopathies and diseases such as stroke and myocardial infarction.

Methods

Mice

Conditional *Bax* mice (78), *Bak* null mice (79), *Tie2-cre* mice (80), *Cdh5(PAC)-creERT2* mice (32), *caspase 8* null mice (81), *Mlkl* null mice (82), *ROSA26*$^{Sortm4(ACTB-tdTomato,-EGFP)Luo}$ (*mTmG*) mice (46) have been previously described. Conditional *Vegfr2* mice crossed with *Tie2-creERT2* have been described previously (39) and show 80% reduction of endothelial VEGFR2 protein along with loss of ECs from non-retinal organs following tamoxifen administration (39, 83). Animals were maintained on an inbred C57BL/6 background. The day of birth was termed P0. Mice of both sexes were used. *Bak*$^{-/-}$*Bax*$^{iEC/iEC}$ mice were injected with 50 µg tamoxifen (MP Biomedicals, dissolved in sterile corn oil + 5% ethanol) by intragastric injection at postnatal day 2 (P2) and P3. For conditional *Vegfr2* mice, tamoxifen (Sigma) was dissolved in ethanol and diluted in sterile corn oil to 1 µg/µL with mice administered 50 µg by intraperitoneal injection at P7, P8 and P9 with eyes dissected for analysis at P10. Control genotypes for experiments involving *Bak*$^{-/-}$*Bax*$^{EC/EC}$ and *Bak*$^{-/-}$*Bax*$^{iEC/iEC}$ mice were: *Bak*$^{-/-}$*Bax*$^{flox/+}$*;cre*$^{+}$*, Bak*$^{-/-}$*Bax*$^{flox/+}$*;cre*$^{-}$ and *Bak*$^{-/-}$*Bax*$^{flox/flox}$*;cre*$^{-}$.

Oxygen-induced retinopathy

Nursing dams with P7 pups were housed in a Perspex chamber (BioSpherix) and exposed continuously to 74±1% oxygen in air maintained by a ProOx110 oxygen controller (BioSpherix). Duration of oxygen exposure and subsequent recovery time in room air is indicated in each figure. Pups were fostered to BALB/c females following exposure to 3 days of high oxygen to prevent oxygen toxicity in dams.

VEGFA and ANG2 neutralisation experiments

Mouse anti-mouse/human VEGFA neutralising antibody B20-4.1.1 (50) (Genentech) and

control mouse anti-human CD8a antibody OKT8 (WEHI Antibody Facility) were administered to mice by intraperitoneal injection at the time points indicated either at 5 mg/kg or at the dose stated in the figure legend. Human anti-mouse/human ANG2 antibody ABA (63) (provided by Gou Young Koh, KAIST, Daejeon) and control human anti-respiratory syncytial virus antibody palivizumab (provided by Steven Stacker, Peter MacCallum Cancer Centre, Melbourne) were administered to mice by intraperitoneal injection at 20 mg/kg at the time points indicated.

Immunohistochemical staining

For whole-mount immunohistochemistry, eyes were fixed for 2 h in 4% paraformaldehyde at 4^{O}C before dissecting and blocking retinas for 1 h at room temperature in Dulbecco's phosphate buffered saline (DPBS) with 1% Triton X-100 and 2% donkey or goat serum. Retinas were stained with primary antibodies prepared in blocking solution overnight at 4˚C, washed in DPBS containing 0.01% Triton X-100, then stained overnight with secondary antibodies prepared in blocking solution. Primary antibodies were rat anti-PECAM1/CD31 (BD Pharmingen, 553370, clone MEC13.3), goat anti-PECAM1/CD31 (R&D Systems, AF3628), goat anti-collagen IV (Merck, AB769), rabbit anti-cleaved (active) caspase 3 (Cell Signaling, 9664, clone 5AE1), rat anti-ICAM2/CD102 (BD Pharmingen, 553326, clone 3C4(mIC2/4)), rat anti-VE cadherin (BD Pharmingen, 555289, clone 11D4.1), rabbit anti-pimonidazole (Hypoxyprobe, PAb2627AP), rabbit anti-NG2 (Merck, AB5320), rabbit anti-ERG (Abcam, ab110639, clone EPR3863), rabbit anti-FLI1 (Abcam, ab15289), rabbit anti-GFAP (DAKO, Z0334), human anti-ANG2 (4H10) (63), rabbit anti-phospho H3 (Ser10) conjugated to AF488 (Merck, 06-570-AF488) and goat anti-ESM1 (R&D Systems, AF1999). Secondary antibodies were donkey anti-rabbit-Cy3

(Jackson, 711-165-152), donkey anti-rabbit-AF647 (Jackson, 711-605-152, donkey anti-rat-DL488 (Jackson, 712-485-153), donkey anti-rat-Cy3 (Jackson, 712-165-150), donkey anti-rat-AF647 (Jackson, 712-605-150), donkey anti-goat-DL405 (Jackson, 705-475-147), donkey anti-goat-Cy3 (Jackson, 705-165-147) and streptavdin-AF488 (Jackson, 016-540-084). For IsolectinB4 (Vector Laboratories, B-1205) staining, retinas were blocked in 1% BSA, 0.3% Triton-X 100 in DPBS then incubated with Isolectin B4 in 0.4% Triton-X 100 in Hank's balanced salt solution. Retinas were incubated in 2 µg/ml Hoechst 33342 (Invitrogen, H3570) in 0.01% Triton-X 100 DPBS for 2 hours at room temperature and imaged same day. Retinas were mounted with Prolong Diamond (Invitrogen, P36961). For hypoxia detection, pups were administered 60 mg/kg pimonidazole (Hypoxyprobe) by intra-peritoneal injection either immediately after exiting the oxygen chamber (30 min labelling duration) or 24 h after exiting the chamber (2 h labelling duration). Pimonidazole was detected using rabbit anti-pimonidazole antibody and staining performed as above. For intravenous lectin perfusion, P7 pups were anaesthetised using Xylazil-20 (20 mg/kg) (Troy laboratories Pty Ltd) and Ketamine (100 mg/kg) (Hospira Australia Pty Ltd) via intraperitoneal injection, then 30 µl of DyLight488-conjugated *Lycopersicon esculentum* lectin (Vector Laboratories, DL-1174) was injected retro-orbitally and allowed to circulate for 2 min before retinas were fixed, dissected and stained as above. In mice subjected to 48 + 24RA, *L. esculentum* lectin was injected intracardially, via the left ventricle. For cryosectioning, P18 retinas were fixed for 24 h, equilibrated in 30% sucrose in DPBS for at least one hour at room temperature and frozen in O.C.T. embedding compound (Scigen). 20 µm cryosections were adhered to polysine slides, washed in DPBS then blocked and stained as for wholemount retinas.

Imaging & image analysis

Retinas were imaged using a Leica TCS SP8 confocal microscope using 10x/0.4 NA, 20x/0.75 NA or 40x/1.30 NA objectives and Leica Application Suite software. All image analysis was performed in the FIJI distribution of ImageJ software (84). Apoptotic ECs (defined as cleaved (active) caspase 3^+/PECAM1$^+$ cells enclosed by collagen IV signal) were quantified manually from confocal z stack images from the central retina at P8 and normalised to central retina area. Central retina vessel area was calculated based on PECAM1 signal from maximum intensity projection images following application of a median filter (2 pixels) and 'despeckle' filter prior to manually adjusting threshold and measuring area. Vessel area was normalised to total area of the central retina. Vessel regression was determined from equivalent areas as a ratio of PECAM1$^+$ vessel segment length to collagen IV$^+$ vessel segment length in a semi-automated fashion. Binary masks of both PECAM1 and collagen IV channel were made by various morphological filters and thresholding signal manually. Collagen IV$^+$ PECAM1$^-$ vessel segment mask (i.e. regressing vessels) was generated by subtracting PECAM1 mask from collagen IV mask. Collagen IV$^+$ PECAM1$^-$ mask and collagen IV mask were then skeletonised and length of vessels within each mask was measured. Collagen IV$^+$ PECAM1$^-$:collagen IV ratio was generated automatically based on vessel length. Data represented as PECAM1:collagen IV ratio. ICAM2:collagen IV ratio was calculated in the same way, replacing PECAM1 with ICAM2 signal. Arterial side branches were counted as perfused if lectin signal overlapped continuously with ICAM2. Number of perfused arterial side branches within the central retina were counted and normalised to artery length. Non-perfused side branches were further categorised as 'attached', 'disrupted' or 'detached' based on ICAM2 signal.

‘Attached’ vessels were not perfused but had normal ICAM2 signal (identical appearance to perfused side branches). ‘Disrupted’ side branches had abnormal ICAM2 morphology compared to normal vessels, suggesting they were in the process of closing their lumen and detaching from the artery. ‘Detached’ side branches did not have continuous ICAM2 signal between side branch and major artery but did have continuous collagen IV signal. EC number was counted within equivalent regions of the same size and normalised to retina area. EC nuclei were counted manually based on Hoechst 33342 or FLI1 nuclei in cells positive for vascular markers (Isolectin B4 or PECAM1). When using Hoechst 33342, NG2 staining was included to exclude pericyte nuclei. Number of FLI1 particles (nuclei) were counted after applying a median filter (2 pixels), removing noise with ‘despeckle’ function and analysing particles greater than 20 square-pixels. Particles were then manually checked through confocal Z-stacks to ensure all EC were counted. EC proliferation was determined by manually counting phospho-histone H3 $(Ser10)^{+}$ $FLI1^{+}$ nuclei and normalised to total EC number in each region of the retina. ECs were then assigned as peripheral or central region based on demarcation described above. Network fragmentation, vessel branch points and vessel width were quantified from PECAM1 images of central retina vasculature. A median filter (2 pixels) was first applied to the PECAM1 images, which were then segmented using the Trainable Weka Segmentation Plugin in FIJI (85). Segmented images were then skeletonised. The number of separate, independent network skeletons was used as a measure of network fragmentation. The number of skeletons and vessel branch points were both normalised to central retina area. Vessel width was calculated as total vessel area divided by total vessel length calculated from Weka segmented images. Hypoxic area in the central retina was quantified from pimonidazole

images. A 20-pixel median filter was applied to the images and a signal intensity threshold used to distinguish hypoxic signal from background. Hypoxic area was normalised to total central retina area. Neovascular tufts were quantified based on maximum intensity projection images of collagen IV signals, with neovascular lesions defined as bright, globular collagen IV+ structures. These were segmented manually in Adobe Photoshop CC 2015 and area calculated in FIJI. Neovascular area per retina was normalised to total retina area. Where necessary, a despeckle filter was applied to select channels in images displayed in figures for clarity.

Retina live-imaging

Bak$^{-/-}$ *Bax*$^{iEC/iEC}$ *mTmG* mice were injected with tamoxifen as described above by intra-gastric injection at P2 and P3. Dam and pups were exposed to high oxygen for 48 h followed by 12 h in room air. Retinas were then dissected immediately in cold DMEM, 5 radial incisions made and then flat-mounted with the internal limiting membrane face-down on a disc of 1% low-melting point agarose gel dissolved in DMEM containing 10% FCS and set in a 35 mm culture dish with cover glass bottom (Eppendorf, 0030740017). Nitex 50 µm filter mesh (Sefar, 03-50/31) dipped in molten 1% agarose/DMEM/10% FCS mixture was laid on top of the retina and allowed to set briefly to minimise retina movement during imaging. The dish was then fixed into in a custom 3D printed stage insert with inbuilt water reservoirs to maintain humidity. Retinas were live-imaged using an inverted Leica SP8 confocal microscope using a HyD detector and a 10x/0.4 NA objective. Retinas were maintained at 37^{O}C and 5% humidified CO_2. Images were acquired every 30 min for 5 h. Post-acquisition, a mean filter (1 pixel) was applied to the images using FIJI software.

VEGFA ELISA

VEGFA levels in whole retina lysates were quantified using a mouse VEGF Quantikine ELISA kit (R&D Systems, MMV00) as per the manufacturer's instructions. Briefly, freshly dissected whole retinas were snap frozen in dry ice, thawed in 50 µl of DPBS and homogenised by manual trituration 20 times. Retina homogenates were subject to two freeze/thaw cycles then centrifuged at 5000 x g for 5 min. An equal volume of lysate was then assayed per retina. VEGFA concentrations were calculated from a standard curve generated by 4-parameter logistic regression analysis in R Version 3.4.4 using the drc package (86).

Statistics

All data are shown as mean ± standard error of the mean (SEM). Statistical analyses were performed for all quantitative data by using Prism 7.0 (Graph Pad) or in R Version 3.4.4 where specified. P-values <0.05 was considered significant.

Study approval

All experiments involving animals were performed with procedures approved by The Walter & Eliza Hall Institute of Medical Research Animal Ethics Committee or with University of Nottingham Animal Welfare and Ethical Review Board approval.

Author Contributions

Z.L.G. performed experiments, analysed data & wrote the manuscript; L.W. developed analytical tools and analysed data; V.H.Y.W., Z.H., B.V.B. performed experiments and analysed data; R.Y.Y., A.R.M., A.V.B. performed experiments; D.O.B. analysed data; K.B. & C.P. advised on live imaging protocol; R.C.A.S. provided essential equipment, conceptual advice and analysed data; L.C. conceived the project, performed experiments, analysed data & wrote the manuscript. All authors contributed to and approved the manuscript.

Acknowledgements

The authors thank Genentech Inc. for generous provision of the B20-4.1.1 antibody, Goh Young Koh (KAIST, Daejeon) for generously providing the anti-ANG2 antibodies ABA and 4H10, Steven A. Stacker (Peter MacCallum Cancer Centre, Melbourne) for provision of the palivizumab antibody, Douglas Green (St Jude Children's Research Hospital, Memphis) for *Bax* conditional allele mice, Masashi Yanagisawa (UT Southwestern) for *Tie2-cre* mice, Razqallah Hakem (University of Toronto) for *caspase 8*$^{-/-}$ mice, Warren Alexander (Walter & Eliza Hall Institute) for *Mlkl*$^{-/-}$ and double knockout *Caspase8*$^{-/-}$*Mlkl*$^{-/-}$ mice, Ralf H. Adams (Max Planck Institute, Münster) for Cdh5(PAC)-creERT2 mice, Glenna-Faye Dabrowski, Melissa Pritchard, Jaclyn Gilbert and Dannielle Cooper for expert animal care, Steven Stacker (Peter MacCallum Cancer Centre), Andreas Strasser (Walter & Eliza Hall Institute), Anne K. Voss (Walter & Eliza Hall Institute) and members of the Development and Cancer Division (Walter & Eliza Hall Institute) for informative discussion. This work was made possible through Victorian State Government Operational Infrastructure Support and Australian Government NHMRC IRIISS. This work was supported by the National Health and Medical Research Council, Australia (Project Grant: 1125536 to L.C.); the Australian Research Council (Future Fellowships: 110100891 to L.C.); Australian Government Research Training Program Scholarship (to Z.L.G.), the L.E.W Carty Charitable Fund (to L.C.); the Medical Research Council (to D.O.B., MR/K013157/1); NIH NEI 1 R21 EY027067-01 (K.B. & C.P.) and the Kjell and Märta Beijer's foundation (to K.B.) and the RMH Neuroscience Foundation. AVB supported by the British Heart Foundation (Grant number PG/18/31/33759 (DOB)); The Royal Society (Grant number RGS\R1\191221 (AVB)).

References

1. Geudens I, and Gerhardt H. Coordinating cell behaviour during blood vessel formation. *Development.* 2011;138(21):4569-83.
2. Betz C, Lenard A, Belting HG, and Affolter M. Cell behaviors and dynamics during angiogenesis. *Development.* 2016;143(13):2249-60.
3. Hellstrom A, Smith LE, and Dammann O. Retinopathy of prematurity. *Lancet.* 2013;382(9902):1445-57.
4. Stitt AW, Curtis TM, Chen M, Medina RJ, McKay GJ, Jenkins A, et al. The progress in understanding and treatment of diabetic retinopathy. *Prog Retin Eye Res.* 2016;51:156-86.
5. Herrington W, Lacey B, Sherliker P, Armitage J, and Lewington S. Epidemiology of Atherosclerosis and the Potential to Reduce the Global Burden of Atherothrombotic Disease. *Circ Res.* 2016;118(4):535-46.
6. Zhang ZG, Zhang L, Jiang Q, Zhang R, Davies K, Powers C, et al. VEGF enhances angiogenesis and promotes blood-brain barrier leakage in the ischemic brain. *J Clin Invest.* 2000;106(7):829-38.
7. Miller JW, Le Couter J, Strauss EC, and Ferrara N. Vascular endothelial growth factor a in intraocular vascular disease. *Ophthalmology.* 2013;120(1):106-14.
8. Sivaprasad S, Prevost AT, Vasconcelos JC, Riddell A, Murphy C, Kelly J, et al. Clinical efficacy of intravitreal aflibercept versus panretinal photocoagulation for best corrected visual acuity in patients with proliferative diabetic retinopathy at 52 weeks (CLARITY): a multicentre, single-blinded, randomised, controlled, phase 2b, non-inferiority trial. *Lancet.* 2017;389(10085):2193-203.
9. Writing Committee for the Diabetic Retinopathy Clinical Research N, Gross JG, Glassman AR, Jampol LM, Inusah S, Aiello LP, et al. Panretinal Photocoagulation vs Intravitreous Ranibizumab for Proliferative Diabetic Retinopathy: A Randomized Clinical Trial. *JAMA.* 2015;314(20):2137-46.
10. Mintz-Hittner HA, Kennedy KA, Chuang AZ, and Group B-RC. Efficacy of intravitreal bevacizumab for stage 3+ retinopathy of prematurity. *N Engl J Med.* 2011;364(7):603-15.
11. Good WV, and Early Treatment for Retinopathy of Prematurity Cooperative G. Final results of the Early Treatment for Retinopathy of Prematurity (ETROP) randomized trial. *Trans Am Ophthalmol Soc.* 2004;102:233-48; discussion 48-50.
12. Campochiaro PA, Brown DM, Awh CC, Lee SY, Gray S, Saroj N, et al. Sustained benefits from ranibizumab for macular edema following central retinal vein occlusion: twelve-month outcomes of a phase III study. *Ophthalmology.* 2011;118(10):2041-9.
13. Hartnett ME, and Penn JS. Mechanisms and management of retinopathy of prematurity. *N Engl J Med.* 2012;367(26):2515-26.
14. Danis RP, and Wallow IH. HRP/trypsin technique for studies of the retinal vasculature. *Invest Ophthalmol Vis Sci.* 1986;27(3):434-7.
15. Frangieh GT, Green WR, Barraquer-Somers E, and Finkelstein D. Histopathologic study of nine branch retinal vein occlusions. *Arch Ophthalmol.* 1982;100(7):1132-40.

16. Czabotar PE, Lessene G, Strasser A, and Adams JM. Control of apoptosis by the BCL-2 protein family: implications for physiology and therapy. *Nat Rev Mol Cell Biol.* 2014;15(1):49-63.
17. Watson EC, Grant ZL, and Coultas L. Endothelial cell apoptosis in angiogenesis and vessel regression. *Cellular and molecular life sciences : CMLS.* 2017;74(24):4387-403.
18. Korn C, and Augustin HG. Mechanisms of Vessel Pruning and Regression. *Dev Cell.* 2015;34(1):5-17.
19. Mizutani M, Kern TS, and Lorenzi M. Accelerated death of retinal microvascular cells in human and experimental diabetic retinopathy. *J Clin Invest.* 1996;97(12):2883-90.
20. Wei MC, Zong WX, Cheng EH, Lindsten T, Panoutsakopoulou V, Ross AJ, et al. Proapoptotic BAX and BAK: a requisite gateway to mitochondrial dysfunction and death. *Science.* 2001;292(5517):727-30.
21. Watson EC, Whitehead L, Adams RH, Dewson G, and Coultas L. Endothelial cell survival during angiogenesis requires the pro-survival protein MCL1. *Cell Death Differ.* 2016;23(8):1371-9.
22. Koenig MN, Naik E, Rohrbeck L, Herold MJ, Trounson E, Bouillet P, et al. Pro-apoptotic BIM is an essential initiator of physiological endothelial cell death independent of regulation by FOXO3. *Cell Death Differ.* 2014;21:1687-95.
23. Wang S, Park S, Fei P, and Sorenson CM. Bim is responsible for the inherent sensitivity of the developing retinal vasculature to hyperoxia. *Dev Biol.* 2011;349(2):296-309.
24. Watson EC, Koenig MN, Grant ZL, Whitehead L, Trounson E, Dewson G, et al. Apoptosis regulates endothelial cell number and capillary vessel diameter but not vessel regression during retinal angiogenesis. *Development.* 2016;143(16):2973-82.
25. Chen Q, Jiang L, Li C, Hu D, Bu JW, Cai D, et al. Haemodynamics-driven developmental pruning of brain vasculature in zebrafish. *PLoS Biol.* 2012;10(8):e1001374.
26. Kochhan E, Lenard A, Ellertsdottir E, Herwig L, Affolter M, Belting HG, et al. Blood flow changes coincide with cellular rearrangements during blood vessel pruning in zebrafish embryos. *PLoS One.* 2013;8(10):e75060.
27. Lenard A, Daetwyler S, Betz C, Ellertsdottir E, Belting HG, Huisken J, et al. Endothelial cell self-fusion during vascular pruning. *PLoS Biol.* 2015;13(4):e1002126.
28. Franco CA, Jones ML, Bernabeu MO, Geudens I, Mathivet T, Rosa A, et al. Dynamic endothelial cell rearrangements drive developmental vessel regression. *PLoS Biol.* 2015;13(4):e1002125.
29. Smith LE, Wesolowski E, McLellan A, Kostyk SK, D'Amato R, Sullivan R, et al. Oxygen-induced retinopathy in the mouse. *Invest Ophthalmol Vis Sci.* 1994;35(1):101-11.
30. Ke FFS, Vanyai HK, Cowan AD, Delbridge ARD, Whitehead L, Grabow S, et al. Embryogenesis and Adult Life in the Absence of Intrinsic Apoptosis Effectors BAX, BAK, and BOK. *Cell.* 2018;173(5):1217-30 e17.

31. Phng LK, Potente M, Leslie JD, Babbage J, Nyqvist D, Lobov I, et al. Nrarp coordinates endothelial Notch and Wnt signaling to control vessel density in angiogenesis. *Dev Cell.* 2009;16(1):70-82.
32. Wang Y, Nakayama M, Pitulescu ME, Schmidt TS, Bochenek ML, Sakakibara A, et al. Ephrin-B2 controls VEGF-induced angiogenesis and lymphangiogenesis. *Nature.* 2010;465(7297):483-6.
33. Naik E, O'Reilly LA, Asselin-Labat ML, Merino D, Lin A, Cook M, et al. Destruction of tumor vasculature and abated tumor growth upon VEGF blockade is driven by proapoptotic protein Bim in endothelial cells. *J Exp Med.* 2011;208(7):1351-8.
34. Gerber HP, Dixit V, and Ferrara N. Vascular endothelial growth factor induces expression of the antiapoptotic proteins Bcl-2 and A1 in vascular endothelial cells. *J Biol Chem.* 1998;273(21):13313-6.
35. Claxton S, and Fruttiger M. Role of arteries in oxygen induced vaso-obliteration. *Exp Eye Res.* 2003;77(3):305-11.
36. Pierce EA, Foley ED, and Smith LE. Regulation of vascular endothelial growth factor by oxygen in a model of retinopathy of prematurity. *Arch Ophthalmol.* 1996;114(10):1219-28.
37. Uemura A, Kusuhara S, Wiegand SJ, Yu RT, and Nishikawa S. Tlx acts as a proangiogenic switch by regulating extracellular assembly of fibronectin matrices in retinal astrocytes. *J Clin Invest.* 2006;116(2):369-77.
38. Simons M, Gordon E, and Claesson-Welsh L. Mechanisms and regulation of endothelial VEGF receptor signalling. *Nat Rev Mol Cell Biol.* 2016;17(10):611-25.
39. Beazley-Long N, Moss CE, Ashby WR, Bestall SM, Almahasneh F, Durrant AM, et al. VEGFR2 promotes central endothelial activation and the spread of pain in inflammatory arthritis. *Brain Behav Immun.* 2018.
40. Pan Q, Chanthery Y, Liang WC, Stawicki S, Mak J, Rathore N, et al. Blocking neuropilin-1 function has an additive effect with anti-VEGF to inhibit tumor growth. *Cancer Cell.* 2007;11(1):53-67.
41. Lobov IB, Cheung E, Wudali R, Cao J, Halasz G, Wei Y, et al. The Dll4/Notch pathway controls postangiogenic blood vessel remodeling and regression by modulating vasoconstriction and blood flow. *Blood.* 2011;117(24):6728-37.
42. Hughes S, and Chang-Ling T. Roles of endothelial cell migration and apoptosis in vascular remodeling during development of the central nervous system. *Microcirculation.* 2000;7(5):317-33.
43. Scott A, and Fruttiger M. Oxygen-induced retinopathy: a model for vascular pathology in the retina. *Eye (Lond).* 2010;24(3):416-21.
44. Lee J, Kim KE, Choi DK, Jang JY, Jung JJ, Kiyonari H, et al. Angiopoietin-1 guides directional angiogenesis through integrin alphavbeta5 signaling for recovery of ischemic retinopathy. *Sci Transl Med.* 2013;5(203):203ra127.
45. Fukushima Y, Okada M, Kataoka H, Hirashima M, Yoshida Y, Mann F, et al. Sema3E-PlexinD1 signaling selectively suppresses disoriented angiogenesis in ischemic retinopathy in mice. *J Clin Invest.* 2011;121(5):1974-85.
46. Muzumdar MD, Tasic B, Miyamichi K, Li L, and Luo L. A global double-fluorescent Cre reporter mouse. *Genesis.* 2007;45(9):593-605.

47. Ehling M, Adams S, Benedito R, and Adams RH. Notch controls retinal blood vessel maturation and quiescence. *Development.* 2013;140(14):3051-61.
48. Pierce EA, Avery RL, Foley ED, Aiello LP, and Smith LE. Vascular endothelial growth factor/vascular permeability factor expression in a mouse model of retinal neovascularization. *Proc Natl Acad Sci U S A.* 1995;92(3):905-9.
49. Aiello LP, Pierce EA, Foley ED, Takagi H, Chen H, Riddle L, et al. Suppression of retinal neovascularization in vivo by inhibition of vascular endothelial growth factor (VEGF) using soluble VEGF-receptor chimeric proteins. *Proc Natl Acad Sci U S A.* 1995;92(23):10457-61.
50. Liang WC, Wu X, Peale FV, Lee CV, Meng YG, Gutierrez J, et al. Cross-species vascular endothelial growth factor (VEGF)-blocking antibodies completely inhibit the growth of human tumor xenografts and measure the contribution of stromal VEGF. *J Biol Chem.* 2006;281(2):951-61.
51. Rocha SF, Schiller M, Jing D, Li H, Butz S, Vestweber D, et al. Esm1 modulates endothelial tip cell behavior and vascular permeability by enhancing VEGF bioavailability. *Circ Res.* 2014;115(6):581-90.
52. del Toro R, Prahst C, Mathivet T, Siegfried G, Kaminker JS, Larrivee B, et al. Identification and functional analysis of endothelial tip cell-enriched genes. *Blood.* 2010;116(19):4025-33.
53. Felcht M, Luck R, Schering A, Seidel P, Srivastava K, Hu J, et al. Angiopoietin-2 differentially regulates angiogenesis through TIE2 and integrin signaling. *J Clin Invest.* 2012;122(6):1991-2005.
54. Park DY, Lee J, Kim J, Kim K, Hong S, Han S, et al. Plastic roles of pericytes in the blood-retinal barrier. *Nat Commun.* 2017;8:15296.
55. Gale NW, Thurston G, Hackett SF, Renard R, Wang Q, McClain J, et al. Angiopoietin-2 is required for postnatal angiogenesis and lymphatic patterning, and only the latter role is rescued by Angiopoietin-1. *Dev Cell.* 2002;3(3):411-23.
56. Hackett SF, Wiegand S, Yancopoulos G, and Campochiaro PA. Angiopoietin-2 plays an important role in retinal angiogenesis. *J Cell Physiol.* 2002;192(2):182-7.
57. Oh H, Takagi H, Suzuma K, Otani A, Matsumura M, and Honda Y. Hypoxia and vascular endothelial growth factor selectively up-regulate angiopoietin-2 in bovine microvascular endothelial cells. *J Biol Chem.* 1999;274(22):15732-9.
58. Mandriota SJ, and Pepper MS. Regulation of angiopoietin-2 mRNA levels in bovine microvascular endothelial cells by cytokines and hypoxia. *Circ Res.* 1998;83(8):852-9.
59. Pichiule P, Chavez JC, and LaManna JC. Hypoxic regulation of angiopoietin-2 expression in endothelial cells. *J Biol Chem.* 2004;279(13):12171-80.
60. Simon MP, Tournaire R, and Pouyssegur J. The angiopoietin-2 gene of endothelial cells is up-regulated in hypoxia by a HIF binding site located in its first intron and by the central factors GATA-2 and Ets-1. *Journal of cellular physiology.* 2008;217(3):809-18.
61. Kim YH, Choi J, Yang MJ, Hong SP, Lee CK, Kubota Y, et al. A MST1-FOXO1 cascade establishes endothelial tip cell polarity and facilitates sprouting angiogenesis. *Nat Commun.* 2019;10(1):838.

62. Kim J, Kim YH, Kim J, Park DY, Bae H, Lee DH, et al. YAP/TAZ regulates sprouting angiogenesis and vascular barrier maturation. *J Clin Invest.* 2017;127(9):3441-61.
63. Han S, Lee SJ, Kim KE, Lee HS, Oh N, Park I, et al. Amelioration of sepsis by TIE2 activation-induced vascular protection. *Sci Transl Med.* 2016;8(335):335ra55.
64. Gerhardt H, Golding M, Fruttiger M, Ruhrberg C, Lundkvist A, Abramsson A, et al. VEGF guides angiogenic sprouting utilizing endothelial tip cell filopodia. *J Cell Biol.* 2003;161(6):1163-77.
65. Selvam S, Kumar T, and Fruttiger M. Retinal vasculature development in health and disease. *Prog Retin Eye Res.* 2018;63:1-19.
66. Mancuso MR, Davis R, Norberg SM, O'Brien S, Sennino B, Nakahara T, et al. Rapid vascular regrowth in tumors after reversal of VEGF inhibition. *J Clin Invest.* 2006;116(10):2610-21.
67. Baffert F, Le T, Sennino B, Thurston G, Kuo CJ, Hu-Lowe D, et al. Cellular changes in normal blood capillaries undergoing regression after inhibition of VEGF signaling. *Am J Physiol Heart Circ Physiol.* 2006;290(2):H547-59.
68. Xu Q, Wang Y, Dabdoub A, Smallwood PM, Williams J, Woods C, et al. Vascular development in the retina and inner ear: control by Norrin and Frizzled-4, a high-affinity ligand-receptor pair. *Cell.* 2004;116(6):883-95.
69. Rennel ES, Regula JT, Harper SJ, Thomas M, Klein C, and Bates DO. A human neutralizing antibody specific to Ang-2 inhibits ocular angiogenesis. *Microcirculation.* 2011;18(7):598-607.
70. Wang X, Freire Valls A, Schermann G, Shen Y, Moya IM, Castro L, et al. YAP/TAZ Orchestrate VEGF Signaling during Developmental Angiogenesis. *Dev Cell.* 2017;42(5):462-78 e7.
71. Yung YC, Chae J, Buehler MJ, Hunter CP, and Mooney DJ. Cyclic tensile strain triggers a sequence of autocrine and paracrine signaling to regulate angiogenic sprouting in human vascular cells. *Proc Natl Acad Sci U S A.* 2009;106(36):15279-84.
72. Grant ZL, and Coultas L. Growth factor signaling pathways in vascular development and disease. *Growth Factors.* 2019;37(1-2):53-67.
73. Pichol-Thievend C, Betterman KL, Liu X, Ma W, Skoczylas R, Lesieur E, et al. A blood capillary plexus-derived population of progenitor cells contributes to genesis of the dermal lymphatic vasculature during embryonic development. *Development.* 2018;145(10).
74. Stapor PC, Azimi MS, Ahsan T, and Murfee WL. An angiogenesis model for investigating multicellular interactions across intact microvascular networks. *Am J Physiol Heart Circ Physiol.* 2013;304(2):H235-45.
75. Okuno Y, Nakamura-Ishizu A, Otsu K, Suda T, and Kubota Y. Pathological neoangiogenesis depends on oxidative stress regulation by ATM. *Nature medicine.* 2012;18(8):1208-16.
76. Dorrell MI, Aguilar E, Jacobson R, Trauger SA, Friedlander J, Siuzdak G, et al. Maintaining retinal astrocytes normalizes revascularization and prevents vascular pathology associated with oxygen-induced retinopathy. *Glia.* 2010;58(1):43-54.

77. Bucher F, Stahl A, Agostini HT, and Martin G. Hyperoxia causes reduced density of retinal astrocytes in the central avascular zone in the mouse model of oxygen-induced retinopathy. *Mol Cell Neurosci.* 2013;56:225-33.
78. Knudson CM, Tung KS, Tourtellotte WG, Brown GA, and Korsmeyer SJ. Bax-deficient mice with lymphoid hyperplasia and male germ cell death. *Science.* 1995;270(5233):96-9.
79. Lindsten T, Ross AJ, King A, Zong WX, Rathmell JC, Shiels HA, et al. The combined functions of proapoptotic Bcl-2 family members bak and bax are essential for normal development of multiple tissues. *Mol Cell.* 2000;6(6):1389-99.
80. Kisanuki YY, Hammer RE, Miyazaki J, Williams SC, Richardson JA, and Yanagisawa M. Tie2-Cre transgenic mice: a new model for endothelial cell-lineage analysis in vivo. *Dev Biol.* 2001;230(2):230-42.
81. Salmena L, Lemmers B, Hakem A, Matysiak-Zablocki E, Murakami K, Au PY, et al. Essential role for caspase 8 in T-cell homeostasis and T-cell-mediated immunity. *Genes Dev.* 2003;17(7):883-95.
82. Murphy JM, Czabotar PE, Hildebrand JM, Lucet IS, Zhang JG, Alvarez-Diaz S, et al. The pseudokinase MLKL mediates necroptosis via a molecular switch mechanism. *Immunity.* 2013;39(3):443-53.
83. Ved N, Da Vitoria Lobo ME, Bestall SM, C LV, Beazley-Long N, Ballmer-Hofer K, et al. Diabetes-induced microvascular complications at the level of the spinal cord; a contributing factor in diabetic neuropathic pain. *J Physiol.* 2018.
84. Schindelin J, Arganda-Carreras I, Frise E, Kaynig V, Longair M, Pietzsch T, et al. Fiji: an open-source platform for biological-image analysis. *Nature methods.* 2012;9(7):676-82.
85. Arganda-Carreras I, Kaynig V, Rueden C, Eliceiri KW, Schindelin J, Cardona A, et al. Trainable Weka Segmentation: a machine learning tool for microscopy pixel classification. *Bioinformatics.* 2017;33(15):2424-6.
86. Ritz C, Baty F, Streibig JC, and Gerhard D. Dose-Response Analysis Using R. *PLoS One.* 2015;10(12):e0146021.

Figure 1

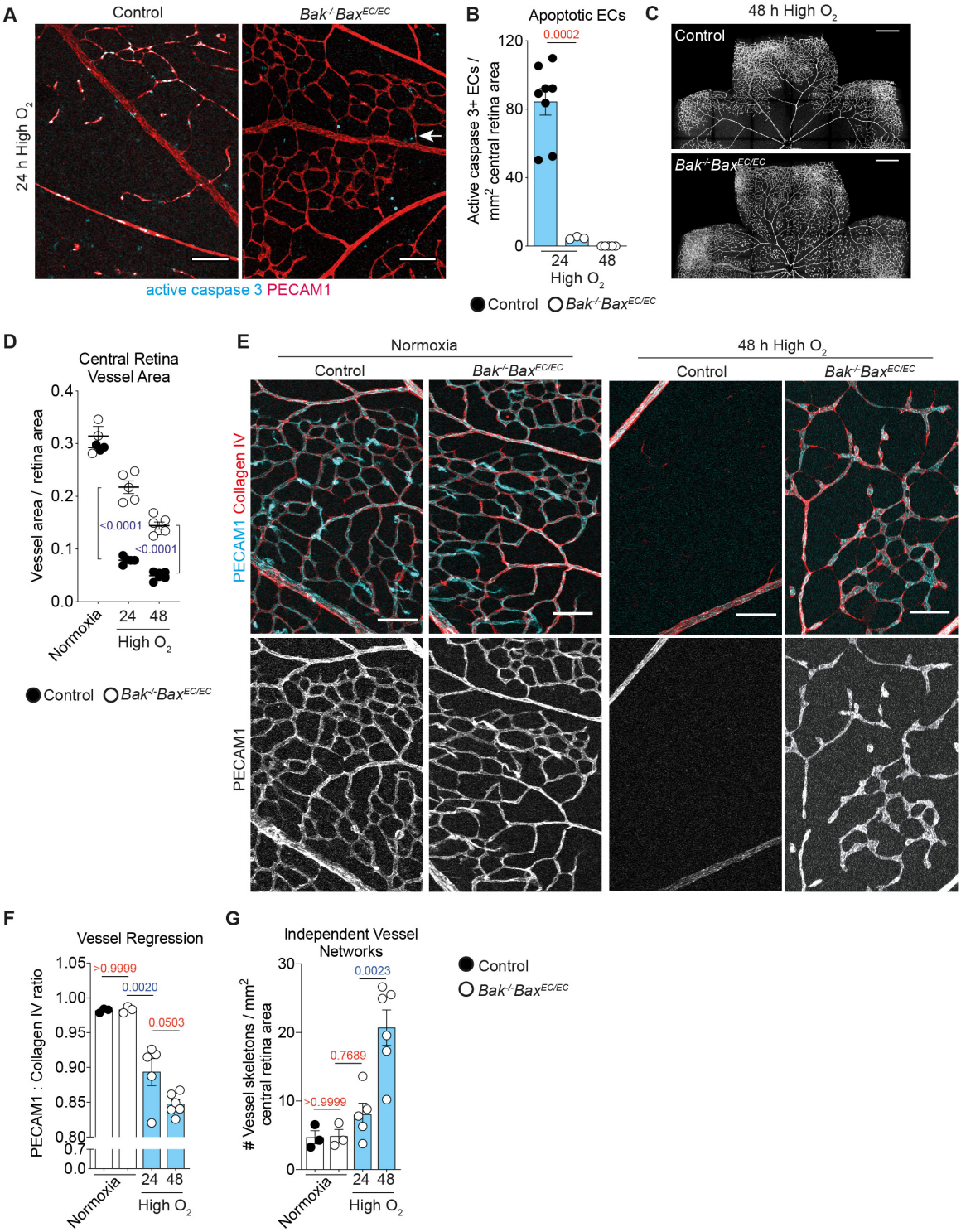

Figure 1. Blocking apoptosis prevents the loss of ECs from retinas exposed to high oxygen. (**A** and **B**) Representative images and quantification of EC apoptosis visualised by active caspase 3 staining (cyan) and PECAM1 (red) in control (n = 8) and *Bak*$^{-/-}$*Bax*$^{EC/EC}$ (24 h: n = 3, 48 h: n = 5) retinas after 24 h or 48 h in high oxygen. Quantitative data from

control mice exposed to high oxygen for 48 h is not shown because there are no central retina capillaries remaining. Arrow indicates rare apoptotic EC in *Bak*$^{-/-}$*Bax*$^{EC/EC}$ retina. Scale bar = 100 μm. Student's two-tailed t-test. (**C**) PECAM1 staining of control and *Bak*$^{-/-}$*Bax*$^{EC/EC}$ retinas after 48 h in high oxygen, scale bar = 500 μm. (**D**) Quantification of central retina vessel area in mice exposed to high oxygen for 24 h (control n = 4, *Bak*$^{-/-}$*Bax*$^{EC/EC}$ n = 5) or 48 h (control n = 6, *Bak*$^{-/-}$*Bax*$^{EC/EC}$ n = 6) compared to 8 day old normoxic mice (control n = 3, *Bak*$^{-/-}$*Bax*$^{EC/EC}$ n = 3). Multiple t-tests using Holm-Sidak correction for multiple comparisons. (**E**) PECAM1 (cyan) and collagen IV (red) staining within the central retina of control and *Bak*$^{-/-}$*Bax*$^{EC/EC}$ mice raised in room air (normoxia) or for 48 h in high oxygen, scale bar = 80 μm. (**F** and **G**) Quantification of vessel regression and network fragmentation in the central retina of *Bak*$^{-/-}$*Bax*$^{EC/EC}$ mice exposed to high oxygen for 24 h (n = 5) or 48 h (n = 6) compared to 8 day old normoxic mice (control n = 3, *Bak*$^{-/-}$*Bax*$^{EC/EC}$ n = 3). Quantitative data from control mice exposed to high oxygen is not shown because there are no central retina capillaries remaining. One-way ANOVA with Tukey's multiple comparisons test. All data are mean ± SEM. Each circle represents one animal.

Figure 2

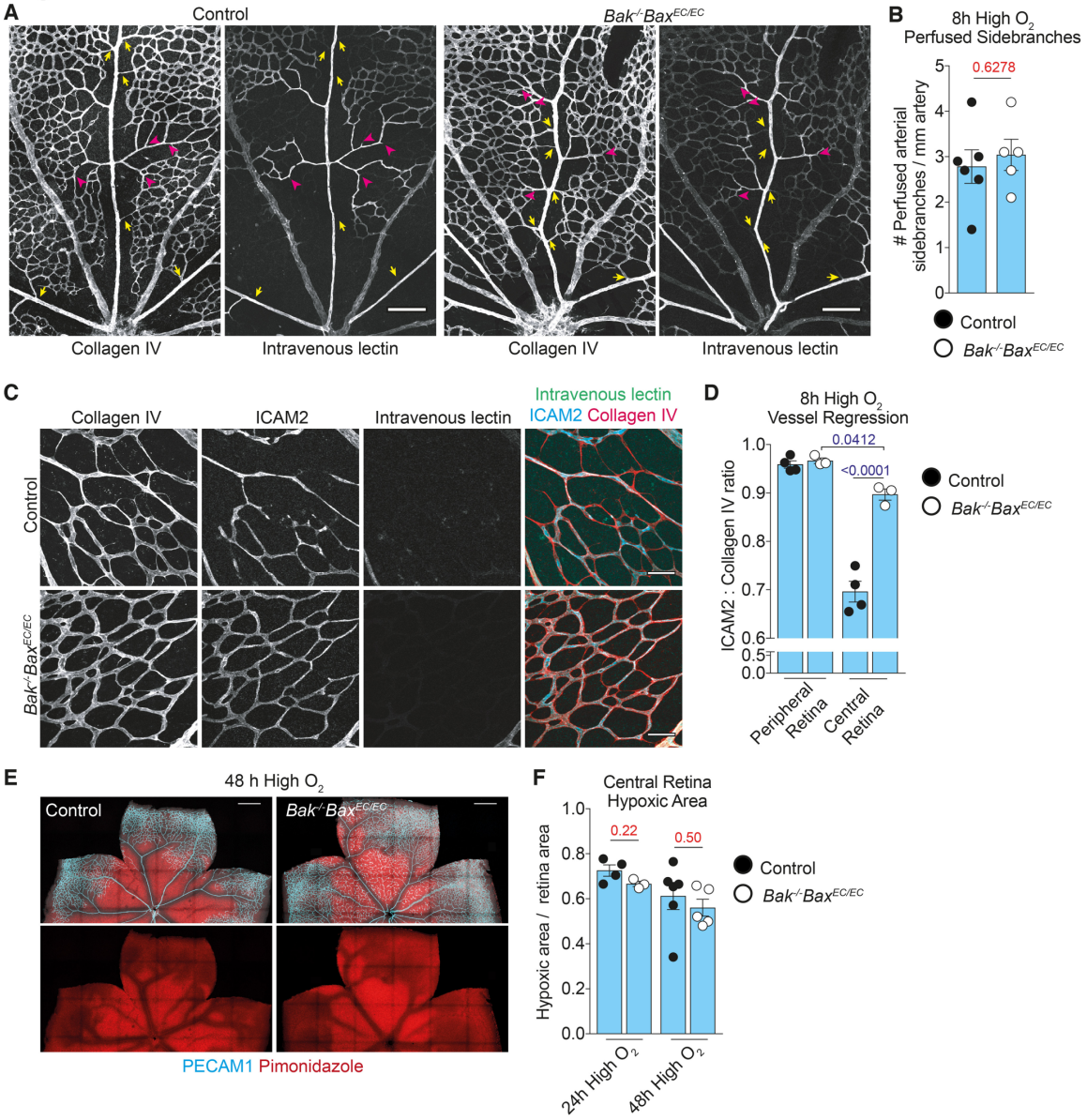

Figure 2. Blocking apoptosis delays, but does not prevent vessel regression. (**A**) Collagen IV and perfused lectin staining in control and *Bak*$^{-/-}$*Bax*$^{EC/EC}$ central retinas. Yellow arrows indicate arterial side branch closure, pink arrowheads indicate representative down-stream vessel closure points. Scale bar = 100 µm. (**B**) Perfused arterial side branches in control (n = 6) and *Bak*$^{-/-}$*Bax*$^{EC/EC}$ mice (n = 5). Student's two-tailed t-test. (**C**) Representative regions of non-perfused capillaries from the central retinas of control and *Bak*$^{-/-}$*Bax*$^{EC/EC}$ mice stained for collagen IV (red), ICAM2 (cyan) and perfused lectin (green). Scale bar = 50 µm. (**D**) Vessel regression in the peripheral and central retina capillaries from control (n = 4) and *Bak*$^{-/-}$*Bax*$^{EC/EC}$ (n = 3) mice. Two-way ANOVA using Tukey's multiple comparisons test. (**E**) Hypoxia visualised by pimonidazole (red) staining and ECs by PECAM1 (cyan) in control and *Bak*$^{-/-}$*Bax*$^{EC/EC}$ retinas following 48 h of high oxygen exposure. Scale bar = 500 µm. (**F**) Central retina hypoxic area in mice exposed to high oxygen for 24 h (control n = 4, *Bak*$^{-/-}$*Bax*$^{EC/EC}$ n = 3) or 48 h (control n = 6, *Bak*$^{-/-}$

Bax$^{EC/EC}$ n = 5). Multiple t-tests using Holm-Sidak correction for multiple comparisons. Animals in panels *A-D* were exposed to high oxygen for 8 h. All data are mean ± SEM. Each circle represents one animal.

Figure 3

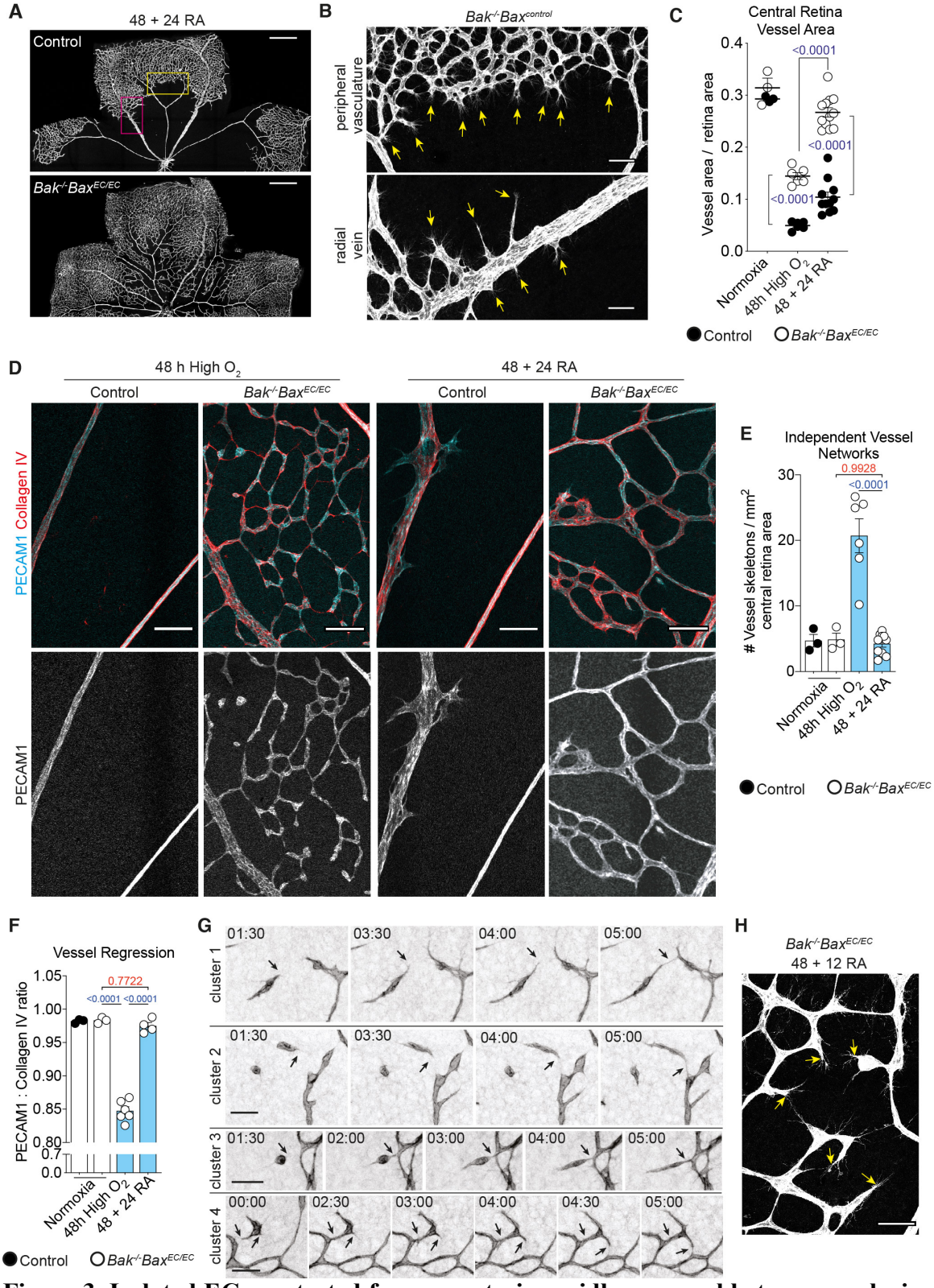

Figure 3. Isolated ECs protected from apoptosis rapidly reassemble to revascularize hypoxic retinas. (**A** and **B**) PECAM1 staining of control and *Bak*$^{-/-}$*Bax*$^{EC/EC}$ retinas

exposed to high oxygen for 48 h followed by 24 h in room air (48 + 24 RA). Scale bars: *A* = 500 µm, *B* = 60 µm. Arrows indicate sprouting vessels. Boxes enlarged in *B* (yellow above, pink below). (**C**) Vessel area in 48+ 24 RA control (n = 11) and *Bak*$^{-/-}$*Bax*$^{EC/EC}$ (n = 12) central retinas. Data for normoxic mice or mice exposed to high oxygen for 48 h from Figure 1D are included for comparison. Two-way ANOVA using Tukey's multiple comparisons test. (**D**) Central retinal vasculature from control and *Bak*$^{-/-}$*Bax*$^{EC/EC}$ mice exposed to 48 h high oxygen or 48 + 24 RA stained for collagen IV (red) and PECAM1 (cyan). Scale bar = 80 µm. (**E** and **F**) Network fragmentation (n = 10) and vessel regression (n = 4) in 48 + 24 RA *Bak*$^{-/-}$*Bax*$^{EC/EC}$ central retinas. Data for normoxic mice or mice exposed to 48 h of high oxygen from Figure 1F & G are included for comparison. One-way ANOVA with Tukey's multiple comparisons test. Quantitative data from control mice exposed to high oxygen is not shown because there are no central retina capillaries remaining. (**G**) Static images from live-imaging retinal explants showing vessels reassembling starting 12 h after return to room air following 48 h exposure to high oxygen. Four independent clusters are shown. Time stamp is hh:mm (t0 = 12 h after return to room air). Arrows indicate where sprouts form new connections. Scale bar = 50 µm. (**H**) Sprouting clusters from a 48 + 12 RA *Bak*$^{-/-}$*Bax*$^{EC/EC}$ retina, scale bar = 50 µm. Arrows indicate filopodial projections. All data are mean ± SEM. Each circle represents one animal.

Figure 4.

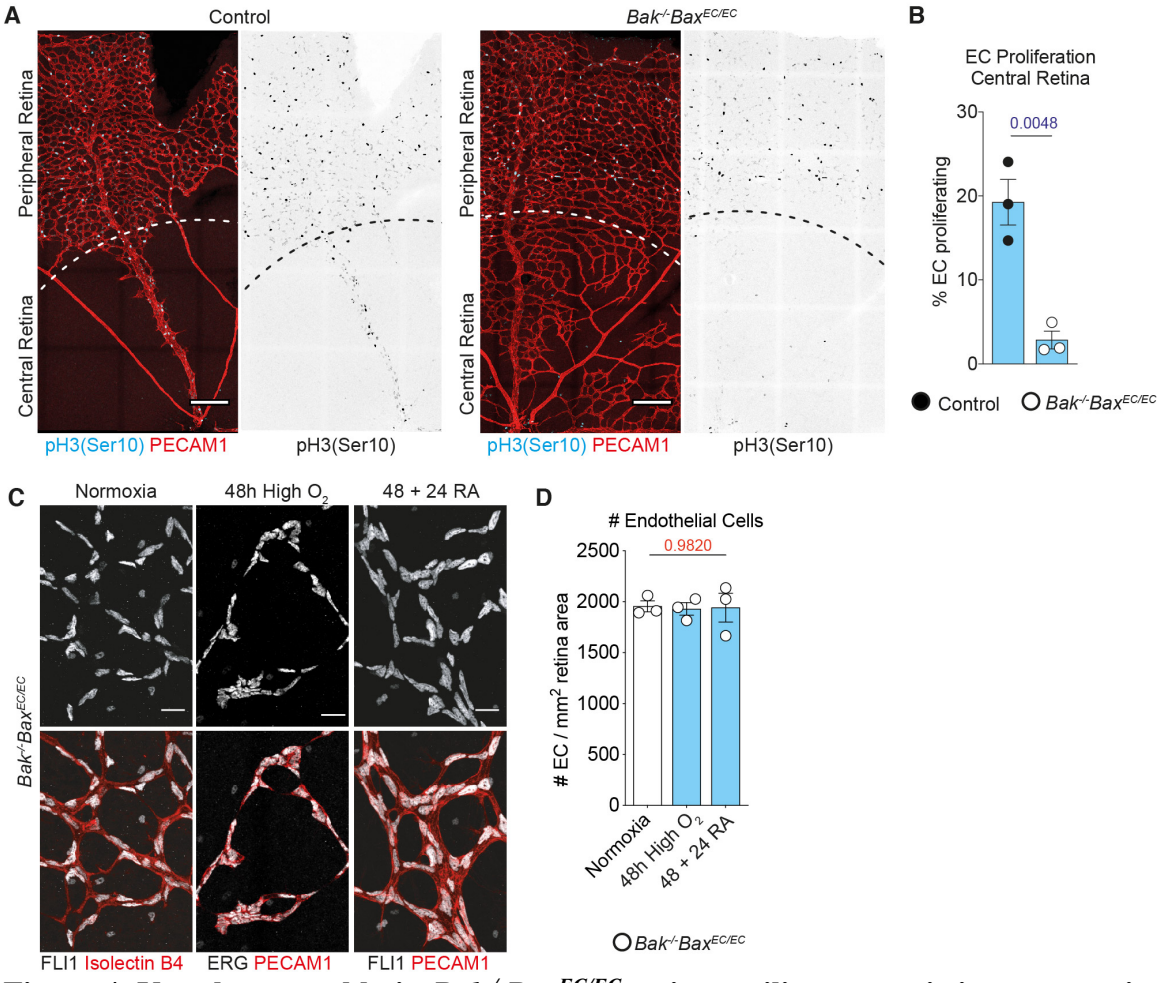

Figure 4. Vessel reassembly in *Bak*$^{-/-}$*Bax*$^{EC/EC}$ retinas utilises pre-existing, apoptosis-protected ECs (**A**) EC proliferation in 48 + 24 RA control and *Bak*$^{-/-}$*Bax*$^{EC/EC}$ retinas visualised by staining for pH3(Ser10) (cyan) and PECAM1 (red). Dotted line demarcates boundary between peripheral and central retina. Scale bar = 200 µm. (**B**) Quantification of proliferating ECs within central retina of 48 + 24 RA control (n = 3) and *Bak*$^{-/-}$*Bax*$^{EC/EC}$ (n = 3) mice. Student's two-tailed t-test. (**C** and **D**) Representative images and quantification of EC number in *Bak*$^{-/-}$*Bax*$^{EC/EC}$ central retina vessels from normoxic mice (n = 3) or mice exposed to 48 h high oxygen alone (n = 3) or with 24 h recovery in room air (48 + 24 RA) (n = 3). EC number quantified based on EC nuclei (co-staining of FLI1 or ERG with EC markers PECAM1 or isolectin B4). Quantitative data from control mice is not shown because there are no central retina capillaries remaining following exposure to high oxygen. Scale bar = 20µm. One-way ANOVA. All data are mean ± SEM. Each circle represents one animal.

Figure 5.

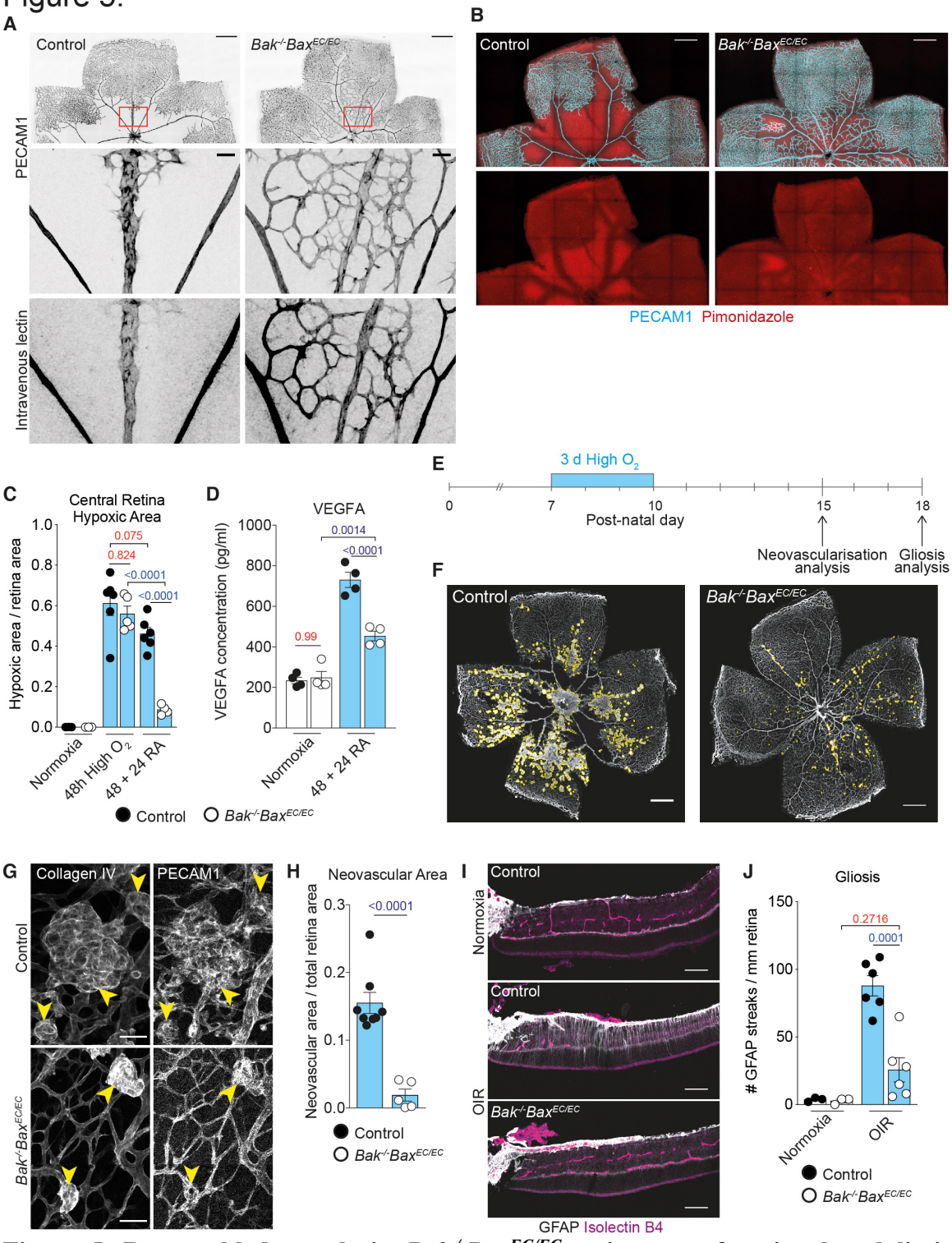

Figure 5. Reassembled vessels in *Bak*$^{-/-}$*Bax*$^{EC/EC}$ retinas are functional and limit neovascularisation and retinal injury. (**A**) 48 + 24 RA control and *Bak*$^{-/-}$*Bax*$^{EC/EC}$ retinas intravenously perfused with lectin and stained for PECAM1. (**B**) Hypoxia visualised by pimonidazole (red) staining (co-stained with PECAM1, cyan) in control and *Bak*$^{-/-}$*Bax*$^{EC/EC}$ retinas exposed to high oxygen for 48 h followed by 24 h in room air (48 + 24 RA). Scale

bar = 500 µm. (**C**) Central retina hypoxia in P8 normoxic mice (control n = 3, *Bak*$^{-/-}$*Bax*$^{EC/EC}$ n = 3), following 48 h in high oxygen (control n = 6, *Bak*$^{-/-}$*Bax*$^{EC/EC}$ n = 5) or 48 + 24 RA (control n = 6, *Bak*$^{-/-}$*Bax*$^{EC/EC}$ n = 4). Two-way ANOVA using Tukey's multiple comparisons test. (**D**) Quantification of VEGFA protein in whole retina extracts from 48 + 24 RA control (n = 4) and *Bak*$^{-/-}$*Bax*$^{EC/EC}$ (n = 4) mice and age-matched normoxic controls (control n = 4, *Bak*$^{-/-}$*Bax*$^{EC/EC}$ n = 4). Two-way ANOVA using Tukey's multiple comparisons test. (**E**) Experimental overview of OIR procedure used in *F – J*. (**F, G, H**) Representative examples and quantification of neovascular area in P15 control (n = 8) and *Bak*$^{-/-}$*Bax*$^{EC/EC}$ (n = 5) retinas stained for collagen IV and PECAM1. Yellow lines outline neovascular lesions (*G*), arrowheads indicate glomerular-like lesions (*H*). Scale bar = 500 µm (*G*) and 50 µm (*H*). Student's two-tailed t-test. (**I** and **J**) Representative images and quantification of Müller cell gliosis visualised by GFAP (grey) staining comparing mice subjected to the OIR (control n = 6, *Bak*$^{-/-}$*Bax*$^{EC/EC}$ n = 6) or age-matched controls raised in room air (normoxia, control n = 2, *Bak*$^{-/-}$*Bax*$^{EC/EC}$ n = 2). Isolectin B4 labels ECs (magenta). Scale bar = 100 µm. Two-way ANOVA with Tukey's multiple comparisons test. All data are mean ± SEM. Each circle represents one animal.

Figure 6.

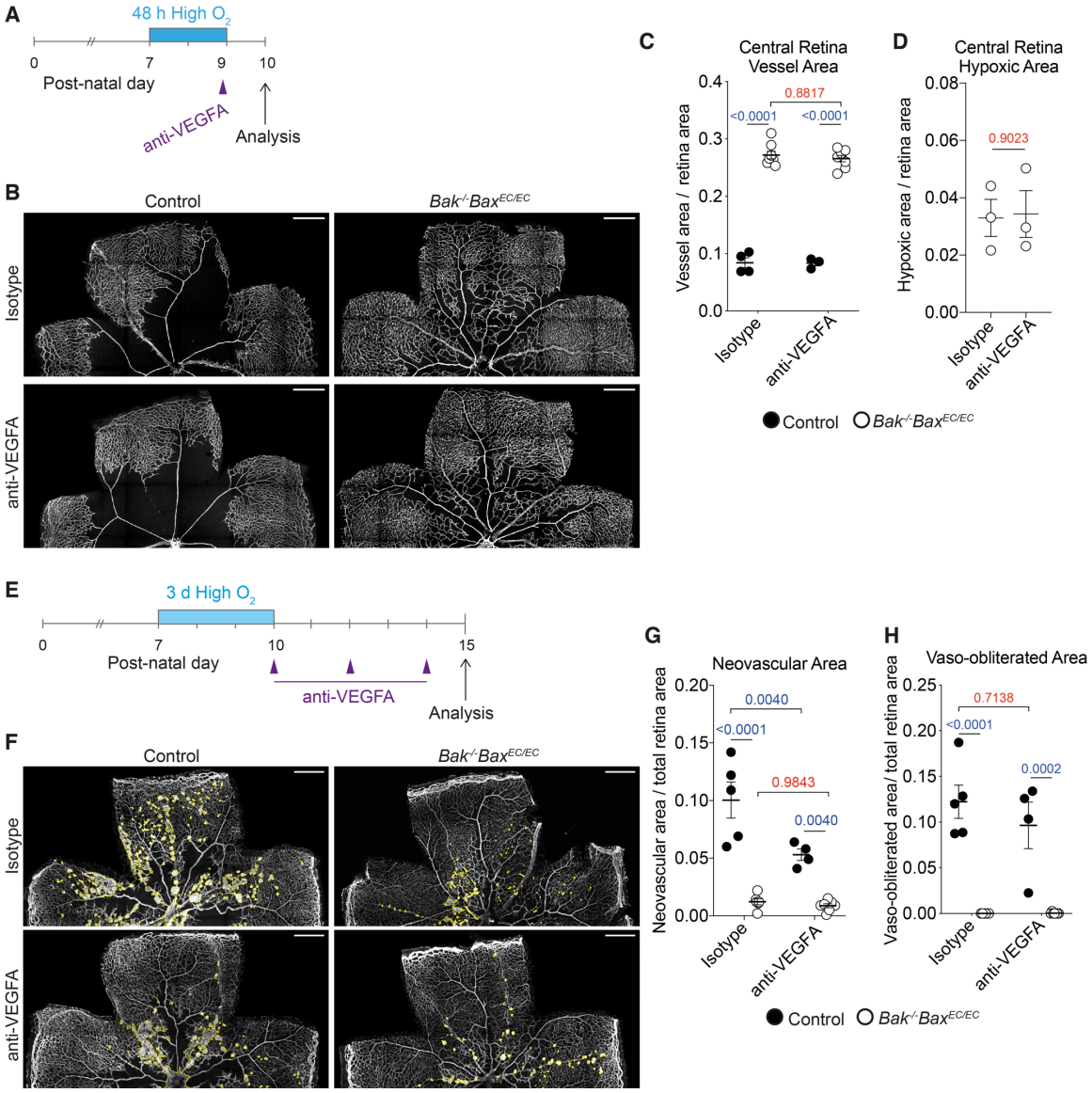

Figure 6. Vessel reassembly is insensitive to VEGFA neutralisation. (**A**) Experimental overview of mice analysed in *B* - *D*. (**B** and **C**) Representative images and quantification of central retinal vasculature in mice subjected to the time course shown in *A* and treated with isotype control (control n = 4, *Bak*$^{-/-}$*Bax*$^{EC/EC}$ n = 8) or anti-VEGFA (control n = 3, *Bak*$^{-/-}$*Bax*$^{EC/EC}$ n = 8). Stained for PECAM1. Scale bar = 500 µm. Two-way ANOVA with Tukey's multiple comparisons test. (**D**) Quantification of central retina hypoxic area in *Bak*$^{-/-}$*Bax*$^{EC/EC}$ mice subjected to the time course shown in *A* and rerated with isotype control (n = 3) or anti-VEGFA (n = 3). Student's two-tailed t-test. (**E**) Experimental overview of mice analysed in *F – H*. (**F**) Representative examples of neovascularisation (yellow outline) in control and *Bak*$^{-/-}$*Bax*$^{EC/EC}$ retinas treated with anti-VEGFA or isotype control antibodies. Scale bar = 500 µm. (**G**) Quantification of neovascular area in retinas from control (isotype n = 5, anti-VEGFA n = 4) and *Bak*$^{-/-}$*Bax*$^{EC/EC}$ mice (isotype n = 6 & anti-VEGFA n = 7). Two-way ANOVA with Tukey's multiple comparisons test. (**H**) Quantification of vaso-obliterated area in retinas from control (isotype n = 5, anti-VEGFA n = 4) and *Bak*$^{-/-}$

Bax$^{EC/EC}$ mice (isotype n = 6 & anti-VEGFA n = 7). Two-way ANOVA with Tukey's multiple comparisons test. All data are mean ± SEM. Each circle represents one animal.

Figure 7.

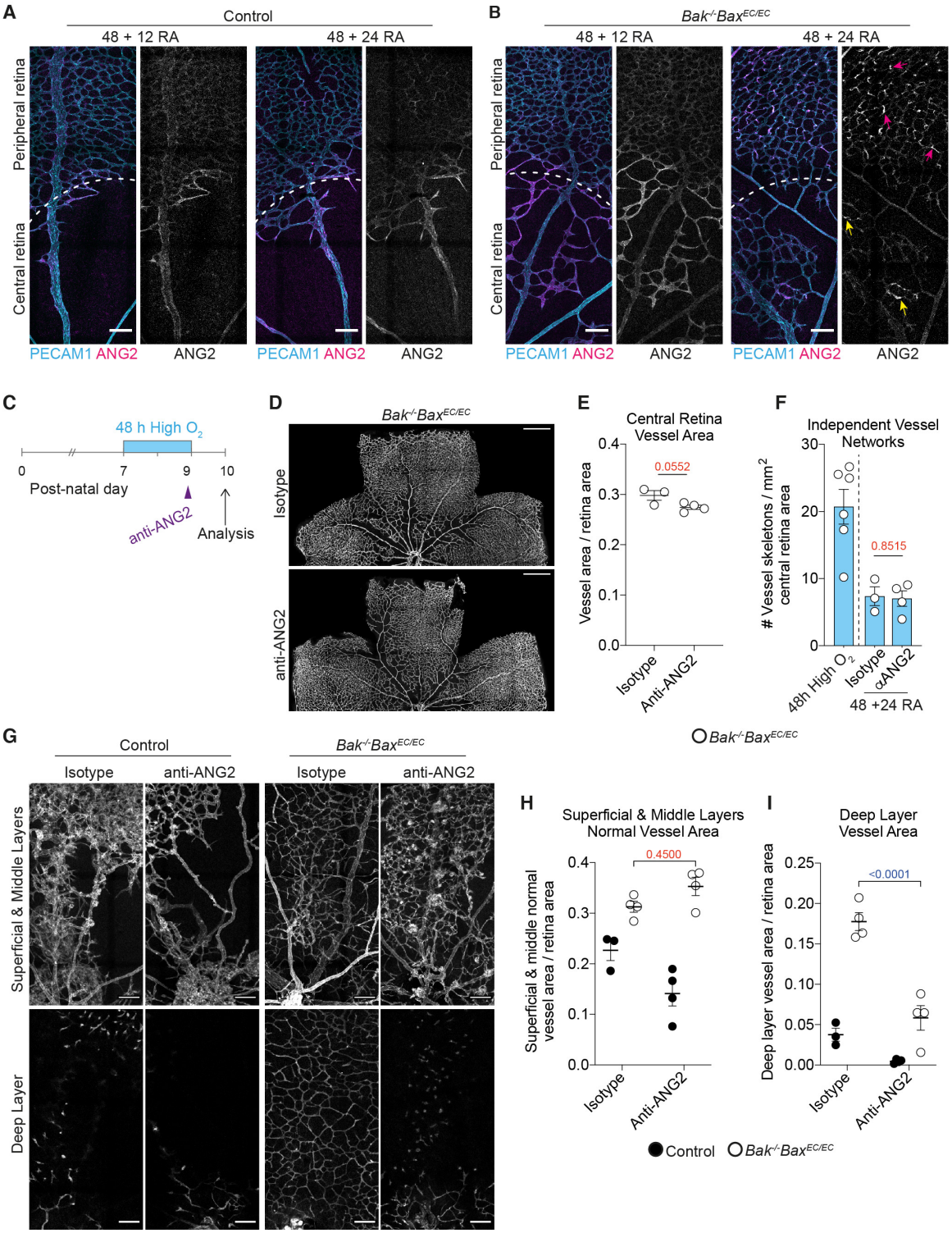

Figure 7. ANG2 is not required for vessel reassembly but required for expansion of reassembled network.

(**A** and **B**) Representative images of ANG2 (magenta, grey) expression in control and *Bak*$^{-/-}$*Bax*$^{EC/EC}$ retinas exposed to high oxygen for 48 h followed by return to room air for 12

(+12 RA) or 24 h (+ 24 RA). Co-stained with PECAM1 (cyan). Pink arrows indicate ANG2+ downwards sprouts, yellow arrows indicate patches of ANG2+ vessels. Scale bar = 100 μm. (**C**) Experimental overview of mice analysed in *D* - *F*. (**D** and **E**) Representative images and quantification of central retinal vasculature in *Bak*$^{-/-}$*Bax*$^{EC/EC}$ mice subjected to the time course shown in *A* and treated with isotype control (n = 3) or anti (α)-ANG2 (n = 4). Stained for PECAM1. Scale bar = 500 μm. Student's two-tailed t-test. (**F**) Quantification of network fragmentation in the central retina of *Bak*$^{-/-}$*Bax*$^{EC/EC}$ mice subjected to the time course shown in *A* and treated with isotype control (n = 3) or anti-ANG2 (n = 4). Data for *Bak*$^{-/-}$*Bax*$^{EC/EC}$ mice exposed to 48 h of high oxygen from Figure 1G are shown for comparison. Student's two-tailed t-test.(**G – I**) Representative images and quantification of vascular area in separate layers from the same field of view of the central retinas of control (isotype control n = 3, anti-ANG2 n = 4) and *Bak*$^{-/-}$*Bax*$^{EC/EC}$ mice (isotype control n = 4, anti-ANG2 n = 4). Scale bar = 100 μm. Two-way ANOVA with Tukey's multiple comparisons test. All data are mean ± SEM. Each circle represents one animal.